8TH URV DOCTORAL WORKSHOP IN COMPUTER SCIENCE AND MATHEMATICS

Edited by
Maria Bras Amorós and Oriol Farràs Ventura

UNIVERSITAT ROVIRA i VIRGILI

Title: 8th URV Doctoral Workshop in Computer Science and Mathematics
Editors: Maria Bras Amorós, Oriol Farràs Ventura
May 2023

Universitat Rovira i Virgili
C/ de l'Escorxador, s/n
43003 – Tarragona
Catalunya (Spain)

ISBN: 978-84-1365-147-7
DOI: 10.17345/9788413651477

CONTENT

PREFACE

This book contains the abstracts of the works presented in the 6th Doctoral Workshop in Computer Science and Mathematics - DCSM 2023. It was celebrated in Universitat Rovira i Virgili (URV), Campus Sescelades, Tarragona, on May 3, 2023. The aim of this workshop is to promote the dissemination of ideas, methods, and results developed by the students of the PhD program in Computer Science and Mathematics from URV. It has been jointly organized by the research group of COPRICA (Codis, Privadesa i Combinatòria Algebraica) and the Doctoral Program on Computer Science and Mathematics of Security of URV.

The editors and organizers invite you to contact the authors for more detailed explanations and we encourage you to send them your suggestions and comments that may certainly help them in the next steps of their PhD thesis. We thank all the participants and, especially, the students that presented their work in this DCSM workshop. Finally, we also want to thank Universitat Rovira i Virgili, the Departament d'Enginyeria Informàtica i Matemàtiques (DEIM), and the Escola Tècnica Superior d'Enginyeria (ETSE) for their support.

Maria Bras Amorós, Oriol Farràs Ventura

Smart Classrooms: Learning Better and Faster through IoT and Artificial Intelligence

Elena Mercedes Figueroa Cabrera *

Smart Technologies Research Group
Department of Computer Engineering and Mathematics
Universitat Rovira i Virgili, Tarragona, Spain
elenamercedes.figueroa@urv.cat

Abstract. Education continues to play a key role that has become crucial in our changing and increasingly complex society. The emerging trend of putting the learner at the centre of the teaching/learning process brings several unprecedented challenges. In parallel, the popularisation of the so-called Internet of Things (IoT) has fuelled a multitude of applications based on the analysis of data using off-the-shelf machine learning techniques. Smart classrooms are physical learning environments that aim at promoting better and faster learning through the use of digital, contextual, and adaptive devices. In this work we review the different aspects to be considered in the smart classroom ecosystem.

Keywords: smart classroom, ambient intelligence, artificial intelligence

1 Introduction

In recent decades, education has undergone a number of fundamental changes aimed at addressing a growing number of challenges: from skill-based focused learning to the adoption of computers and virtual learning environments, the Sustainable Development Goals, and so on. In parallel, concepts such as ambient intelligence (AmI), smart environments or cognitive systems are becoming increasingly important: sensors and real-time analysis of big data can enable applications in a wide range of scenarios, including classrooms.

Today, it is not uncommon to use the Internet and a variety of online information sources to supplement the textbook. Traditional classrooms have become *technology-enriched* classrooms. Yet, so-called smart classrooms are actually technologically enhanced versions of ordinary classrooms.

From our perspective, **smart classrooms** are physical learning environments that implement Koper's proposals for Smarter Leaning Environments (SLEs) to promote better and faster learning through the use of digital, contextual, and adaptive devices [6]. In addition, smart classrooms could help

* PhD advisors: Maria Ferré, Antoni Martínez-Ballesté

analyse relationships between students and even identify specific situations such as bullying or isolation.

It seems like the smart classroom and related proposals will play a key role in future classrooms; however, a number of challenges must be overcome. My PhD research will contribute to applying Information and Communication Technologies (ICT) to classrooms aiming at making teaching and learning more efficient. As an introduction, in this work we sketch an approach to smart classrooms ecosystem.

2 Smart Classrooms

Analysis of the immediate environment (*i.e.* the *context*: lighting, air quality, acoustics, etc.) and assessment of emotions (both student and teacher) are essential elements of the smart classroom ecosystem. In addition, sustainability and architectural issues must also be considered.

2.1 Analysis of the Context

Monitoring and proactively regulating environmental conditions is one of the applications of AmI that is becoming increasingly important in education. In order to improve student concentration and motivation, and to effectively manage classroom tasks, it is necessary to create the right environmental conditions in the classroom. Therefore, systems must be implemented to seamlessly adjust the physical environment to the comfort level best suited for the group of students or the learning activity being conducted [4]. AmI equips classrooms with sensors and software to support students and teachers through a digitised, context-aware, and adaptive environment.

An example is the ACTUA project [1], which aimed to develop an AmI kit to monitor classroom context. It measures parameters such as air quality, room temperature, humidity, and noise in real time. It also shows the teacher the conditions in the classroom in real time and triggers alarms according to certain rules. Thus, it acts as a RIA (Real-time Instructor Assistant) in terms of context [7].

2.2 Emotions, Engagement and Learning

Placing students at the centre of the teaching/learning process makes it necessary to know them better. Students are far from being *just another brick in the wall* and therefore student-centred approaches must consider a variety of students, each with their own skills, interests and socio-economic situations. Understanding students' emotions, especially during lectures, can foster a positive emotional climate in the classroom and, in turn, improve academic performance [8].

Emotion recognition can be supported by technology: In general, videos can be analysed to detect emotions based on facial expressions and also body postures. However, it may be important to correlate this information with user-centred smart health attributes (e.g., heart rate and skin conductance measured with a wristband [3]) to improve emotion recognition related to learning.

Video analysis has been used to assess attendance (*i.e.*, automatically count those present) and even to measure their engagement (in the sense that a student who yawns or stares at the classroom ceiling is probably not paying attention to the lecture) [5]. In addition, attempts to measure learning engagement using language during student interventions can also be found in the literature [2].

Regarding teachers, the analysis of their emotions while teaching can also be beneficial. Analysis of facial expressions, gait and gestures, and speech would provide valuable information about the quality of teaching. In addition, analysing user-centred data would help identify critical moments and explore connections with student conditions and the environment. Last but not least, it would help prevent burnout.

2.3 Other Aspects

Classrooms are becoming a space not only for listening to the teacher and taking notes, but also for discussion, experimentation, working in groups, etc. The concept of the smart classroom is closely related to this conception of the learning space. The distribution of furniture in a classroom where the teacher is the focus of learning activities is very different from a student-centred learning environment where children can receive information from a variety of sources and engage in skill-based learning activities.

Acoustic conditioning is necessary to absorb noise and prevent reverberation to improve speech transmission and clarity. A lighting system able to adapt to the learning activity at hand, the colours used in the decoration and furniture, the type and arrangement of all elements, the use of sustainable materials... all these aspects contribute to the quality of the learning experience and must therefore be given special consideration when designing a smart classroom.

3 Conclusions

The incorporation of information and communication technologies (ICT) in educational institutions involves a transformation process, to change the traditional classroom into a more intelligent learning environment, which, through the use of digital devices and other technological means, contributes to improvements in the teaching/learning process.

Multiple researchers consider concepts such as Ambient Intelligence (AmI), intelligent environments or cognitive systems, which from the real-time analysis of the data collected in their management allow monitoring, regulate and analyze the environmental conditions, the recognition of emotions related to learning, student motivation, concentration, classroom attendance and in some cases the teacher's behaviour. Nevertheless, the implementation of advanced technologies in the classroom, and the constitution of Smart Classrooms can also project new challenges and research opportunities, such as data security and privacy, hardware and software costs, standardization and integration of technology in smart classrooms, heterogeneity of information sources for both students and teachers, among other challenges.

Therefore, we consider that the creation of a Smart Classroom that responds to the solution of one or more of these challenges can be a very beneficial tool to improve the quality of teaching in the current context. Future research should be planned in this direction.

Acknowledgement. Elena M. Figueroa is supported by Banco Santander under the Martí i Franquès grant number 2021PMF-BS-6.

References

[1] ACTUA: Contextual analysis of the mitigation factors of the transmission of COVID19 in the classroom. `https://actua-urv.cat`. Accessed: 2023-03-13.

[2] Kiavash Bahreini, Rob Nadolski, and Wim Westera. Towards real-time speech emotion recognition for affective e-learning. *Education and Information Technologies*, 21(5):1367–1386, April 2015.

[3] Edgar Batista, M. Angels Moncusi, Pablo López-Aguilar, Antoni Martínez-Ballesté, and Agusti Solanas. Sensors for context-aware smart healthcare: A security perspective. *Sensors*, 21(20), 2021.

[4] Gisela Cebrián, Ramon Palau, and Jordi Mogas. The smart classroom as a means to the development of ESD methodologies. *Sustainability*, 12(7):3010, April 2020.

[5] David Dukić and Ana Sovic Krzic. Real-time facial expression recognition using deep learning with application in the active classroom environment. *Electronics*, 11(8):1240, April 2022.

[6] Rob Koper. Conditions for effective smart learning environments. *Smart Learning Environments*, 1(1), November 2014.

[7] Georgios Mathioudakis, Asterios Leonidis, Maria Korozi, George Margetis, Stavroula Ntoa, Margherita Antona, and Constantine Stephanidis. Ami-ria: Real-time teacher assistance tool for an ambient intelligence classroom. 02 2013.

[8] Jing Tan, Jie Mao, Yizhang Jiang, and Ming Gao. The influence of academic emotions on learning effects: A systematic review. *International Journal of Environmental Research and Public Health*, 18(18), 2021.

Vaccination Strategies for COVID-19 in the Omicron Era: A Mathematical Model Analysis

Piergiorgio Castioni *

Department of Computer Engineering and Mathematics, Universitat Rovira i Virgili Tarragona, Spain
piergiorgio.castioni@urv.cat

1 Introduction

In the late stage of the COVID19 pandemic vaccines have become the main tool to counter the worst drawbacks of the infection, such as the high number of hospitalizations and deaths. A lot of countries have strongly relied on massive vaccinations in order to temper the effects of the epidemics without resort to hard NPIs such as school closures, curfews or lockdowns, which are considered to negatively affect both the economy and public health in the form of the so called "pandemic fatigue".
However all the vaccines currently at our disposal, although very effective in preventing severe symptoms and death and useful to reduce the reproduction number as well, have a limited duration, after which the risk of getting reinfected and even to show severe symptoms start to increase again. This makes it necessary to program the vaccination strategy beforehand and to do it in such a way as to flatten the epidemic curve as much as possible.
That gave us the motivation to develop a complex epidemiological model that could capture both the main features of the propagation of SARS-CoV-2 and the effect that vaccines have on it. We then used this model to run a series of simulations to understand what vaccination campaign is the best one.

2 Methods and Results

The mathematical model that we develop was obtained by further developing the model by Arenas et al. [1]. As in the previous model the population is divided into three age strata (young, adults and older adults), it contained the same compartments and spread among the nodes of a metapopulation network. The difference with the previous model lies in two additional features: first susceptible individuals can get vaccinated; secondly the immunization, coming either from recovery or vaccination, disappears after some time.

* PhD advisor: Alex Arenas, Sergio Gómez

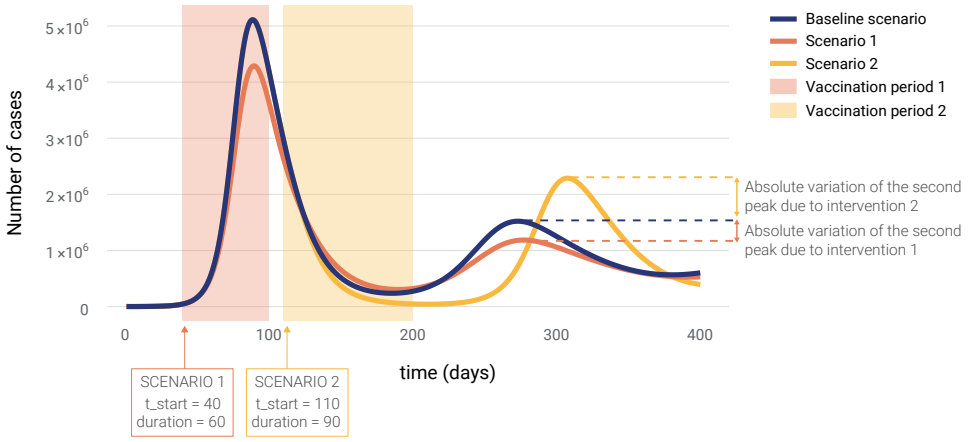

Fig. 1. How the second wave changes if we vaccinate before or after the epidemic peak.

Our purpose was to answer the question of what is the best vaccination strategy in order to contrast the natural decrease in the immunization level. To quantify this we look at the variation in timing and relative height of the second peak of the epidemic for different vaccination scenarios, as well as the relative variation in the cumulative number of hospitalizations and deaths. All those scenarios were then compared with a baseline case produce by our own model without the usage of any vaccination. In order to calibrate some of the parameters we used data from the COVID-19 wave that occurred in Spain between November 2021 and March 2022, which was mainly due to the Omicron variant.

3 Conclusions

Our main results can be summed up in the following way:

1. In general it is better to start the vaccination campaign when the epidemic is rising, because that lowers the risk of having an higher second wave of the infections (see Fig. 1)
2. However if the vaccination campaign starts after the epidemic peak then a longer, more spread-out distribution of doses is to be preferred to a short, concentrated one which, on the contrary, performs better if started before the peak.
3. Prioritizing the vaccination of groups at risk always leads to a lower number of deaths and hospitalizations but can also mean a less effective reduction in the number of cases if they are rising (Fig. 2)

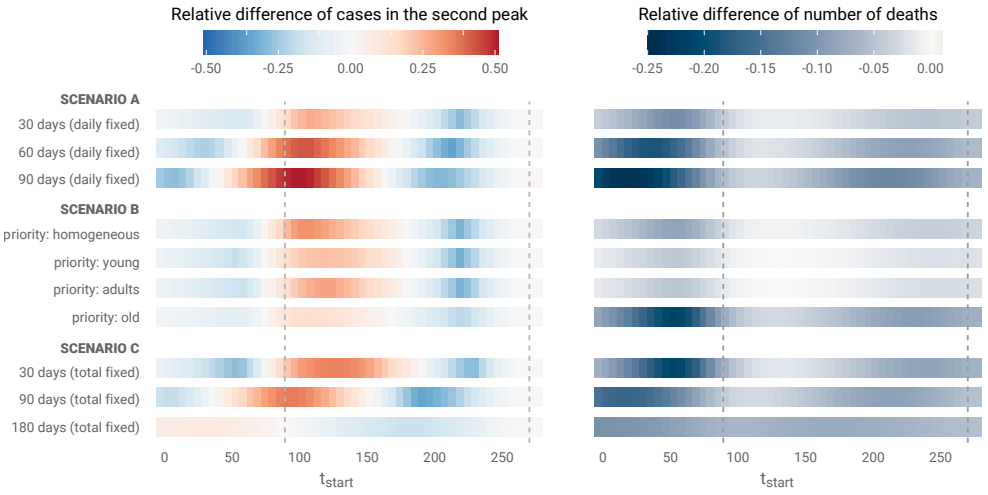

Fig. 2. The height of the second peak (right) and the number of deaths (left) change according to when the vaccination starts and what vaccination strategy we use. On the x-axis there is the starting day of the vaccination measured in days. The variations of cases and deaths are measured relatively to the no-vaccination scenario. In scenarios 1 to 3 the total number of doses is fixed but the duration of the campaign changes; in scenarios 4 to 7 the priority group that gets vaccines faster changes; finally in scenarios 8 to 10 the daily number of doses is fixed and the duration changes.

Our findings could potentially be useful to help policymakers and public health authorities to decide when a vaccination campaign should start in order to minimize the severity of an incoming epidemic wave.

Acknowledgement. My PhD is founded with the FI scholarship, provided by the Secretaría de Universidades e Investigación of the Generalitat de Catalunya through the Agencia de Gestión de Ayudas Universitarias y de Investigación (AGAUR).

References

[1] A. Arenas, W. Cota, J. Gómez-Gardeñes, S. Gómez, C. Granell, J. T. Matamalas, D. Soriano-Paños, and B. Steinegger. Modeling the spatiotemporal epidemic spreading of covid-19 and the impact of mobility and social distancing interventions. *Phys. Rev. X*, 10:041055, Dec 2020.

Prevalence of nonunique dendrograms in agglomerative clustering algorithms

Natàlia Segura-Alabart *

Department of Computer Engineering and Mathematics, Universitat Rovira i Virgili
Tarragona, Spain
natalia.segura@urv.cat

Abstract. Hierarchical clustering is a commonly used data analysis and visualization tool, particularly in the biological field. However, tied distances are a critical challenge to hierarchical clustering, resulting in nonunique dendrograms. To address this challenge, we investigate the prevalence of nonunique dendrograms in microsatellite marker phylogenetic studies using the Unweighted Pair-Group Method with Arithmetic Mean (UPGMA) or the Neighbor-Joining (NJ) method. Our analysis of Scopus database publications indicates that 46% of UPGMA articles and 12% of NJ articles exhibit nonunique clusterings. Our findings highlight the need for solutions to ensure reproducibility and accurate interpretation of results.

1 Introduction

Dendrograms are graphical representations of the hierarchical relationships between the elements of interest and are used in the biological field to analyze genotypes. The proximity of two elements in a dendrogram is indicative of their closeness, as illustrated in Figure 1. Dendrograms are created using hierarchical clustering algorithms.

The Unweighted Pair-Group Method with Arithmetic Mean (UPGMA) [4] and the Neighbor-Joining (NJ) [5,7] are two types of agglomerative clustering algorithms that construct dendrograms from biological data. These distance-based methods combine two clusters or elements into a higher-level one.

During the agglomerative process, identical distance values between different pairs of genotypes or tied values may occur. This situation is known as the ties in proximity problem [1]. It can hinder the clustering method and lead to multiple structurally different hierarchical clusterings, thereby making difficult the reproducibility and interpretation of the results. Figure 1 shows an example where a tie between five elements results in two possible dendrograms.

In this work, we assess the relative frequency of tied distances in dendrograms using either the UPGMA or the NJ method in a representative subset of scientific publications from molecular-marker phylogenetic studies.

* Francesc Serratosa, Alberto Fernández

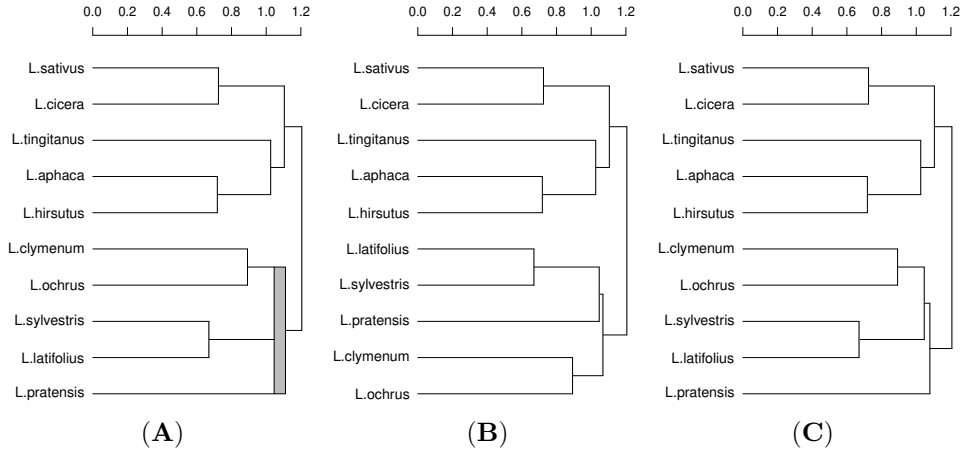

Fig. 1. Example of a dendrogram of genetic distances between 10 individuals created using the UPGMA method, extractred from [6]. (**A**) Dendrogram showing in gray the tied cluster grouping 5 genotypes. (**B, C**) The two possible binary dendrograms, where the last five elements are grouped differently.

2 Methodology

We conducted two Scopus search queries to identify scientific publications related to microsatellite markers up to 2021. We based one search query on the UPGMA method and the other on the NJ method. To retrieve the titles of articles for the UPGMA search query, we used the string shown in [6]. We modified "UPGMA" to ("neighbour joining" OR "neighbor joining" OR "neighbour-joining" OR "neighbor-joining") to retrieve NJ articles. We acquire a UPGMA dataset of 2239 articles and an NJ dataset of 1167 articles. After creating the datasets, we followed the screening process described in [6]; for NJ, we randomly chose 30% of the articles instead of randomly selecting 20%. The data included 102 entries from the UPGMA dataset and 100 from the NJ dataset. We then analyzed these articles to detect ties in their dendrograms using multidendrograms [2] in UPGMA data and MFNJ (multifurcating neighbor-joining) for NJ data [3].

3 Results and Discussion

3.1 Proportion of articles with ties in the hierarchical clustering process

We determined the frequency of ties in the resulting dendrograms among the publications in our sample dataset. We found out that, out of the 102 articles in the UPGMA dataset and the 100 articles in the NJ dataset, there were multiple binary dendrograms in 47 (46% with 95% confidence interval (CI) between 36% and 56%

and 12%) and 12 (12% with 95% CI between 7% and 20%) of those articles, respectively. Thus, using a single arbitrary dendrogram from the different possibilities may be misleading.

Additionally, we investigated the distribution of the number of ties within articles with at least one tie in the resulting dendrogram. As displayed in Figure 2A, most articles in the UPGMA and NJ datasets showed a single tie in their dendrograms, accounting for 53.2% and 75% of cases, respectively. Remarkably, 6.4% of all the articles with ties in the UPGMA dataset (i.e. three) exhibited more than ten ties in their dendrograms.

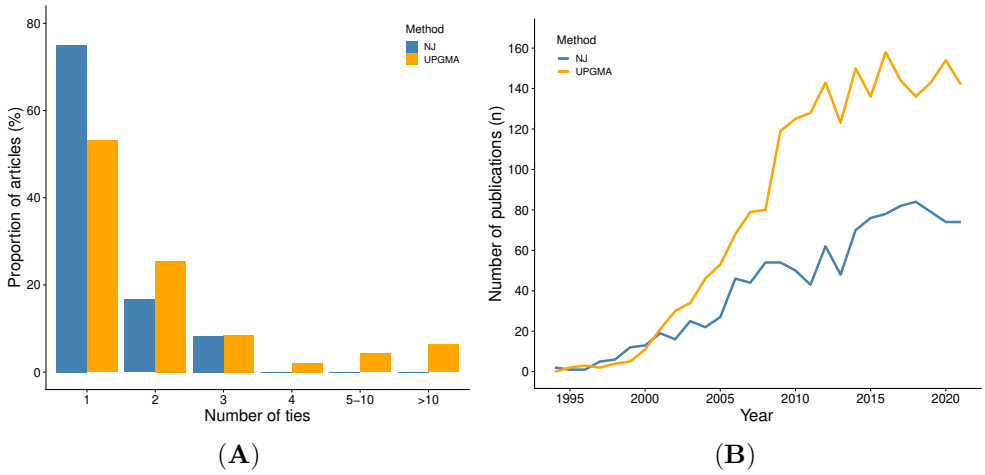

Fig. 2. (**A**) The proportion of articles with at least one tie in their resulting dendrogram using UPGMA (n=47) or NJ (n=12) methods. (**B**) The number of scientific publications that used UPGMA (n=2239) or NJ (n=1167) methods to study microsatellite markers in the Scopus database from 1994 to 2021. In blue is represented NJ data, and in orange is represented UPGMA data.

3.2 Distribution of publications per year

Between 1994 and 2021, authors published the articles included in both datasets (Figure 2B). Both datasets displayed a steady increase in the number of publications since 2000, followed by a plateau in the last ten years. During this plateau phase, the number of articles published yearly for the NJ and UPGMA datasets was more than 70 and 100, respectively. However, the UPGMA dataset doubled the number of articles (n=2239) compared to the NJ dataset (n=1167). This observation suggests that, although both datasets showed a similar trend in the number of publications over time, there has been a greater tendency to use UPGMA compared to NJ in the context of microsatellite marker studies.

4 Conclusions

In this research, we compared the proportion of tied distances observed in scientific publications that had used either the UPGMA or NJ method in molecular-marker phylogenetic studies. Our findings indicate a higher proportion of tied instances in UPGMA data compared to NJ data, at 46% and 12%, respectively. These results highlight the importance of using methods that effectively deal with tied instances to ensure reproducible research and a clear interpretation of the results.

Acknowledgement. This research is supported under the Martí i Franquès fellowship program(2020PMF-PIPF-45) and the PFR program (2019PFR-URV-B2-41), from Universitat Rovira i Virgili .

References

[1] T. Backeljau, L. De Bruyn, H. De Wolf, K. Jordaens, S. Van Dongen and B. Winnepennincks. Multiple UPGMA and neighbor-joining trees and the performance of some computer packages. *Mol Biol Evol.*, 13(2):309-313,1996.

[2] A. Fernández and S. Gómez. Solving non-uniqueness in agglomerative hierarchical clustering using multidendrograms. *J Classif.*, 25:43-65,2008.

[3] A. Fernández, N. Segura-Alabart and F. Serratosa. The multifurcating neighbor-joining algorithm for econstructing n-ary phylogenetic trees. *Manuscript ready for publication submission*,2023.

[4] G.N. Lance and W.T. Williams. A generalized sorting strategy for computer classifications. *Nature.*, 212:218,1966.

[5] N. Saitou and M. Nei. The neighbor-joining method: a new method for reconstructing phylogenetic trees. *Mol Biol Evol.*, 4(4):406-425,1987.

[6] N. Segura-Alabart, F. Serratosa, S. Gómez and A. Fernández. Nonunique UPGMA clusterings of microsatellite markers. *Briefings in Bioinformatics.*, 25(5):bbac312, 2022.

[7] J.A. Studier and K.J. Kepplter. A Note on the Neighbor-Joining Algorithm of Saitou and Neil. *Mol Biol Evol.*, 5(6):729-731,1988.

Towards tissues and FOXP3 nuclei automatic edge detections

Alessio Fiorin *

Department of Computer Engineering and Mathematics, Universitat Rovira i Virgili Tarragona, Spain
Pathology Department, Oncological Pathology and Bioinformatics Research Group, Hospital de Tortosa Verge de la Cinta, ICS, Institut d'Investigació Sanitària Pere Virgili (IISPV), 43500 Tortosa, Tarragona, Spain
alessio.fiorin@estudiants.urv.cat

1 Introduction

Breast cancer is a significant health problem worldwide and is the most common cancer among women. A histopathological examination of breast cancer in tissue slides using hematoxylin-eosin staining is the gold standard for its diagnosis, but additional techniques are required to establish other pathological parameters. Thus, auxiliary techniques such as Immunohistochemistry (IHC) staining are employed to recognize molecular subtypes, the histological grade, the proliferation index, and other histological features of breast cancer based on the presence, abundance, and distribution of antigens within tissues that play as tissue biomarkers. IHC is also used to identify immune markers that play a fundamental role in breast cancer evolution [1]. Among the different types of immune populations, lymphocytes have been raised as one of the immune cells with higher prognostic implications [1]. In the last years, the digitization of tissue slides and their analysis using computational methods have improved the detection and quantification of IHC and other histological stains [2]. The main aim of this research focuses on the comparison of different image analysis techniques used for the detection of tissue and regulatory T lymphocytes boundaries which express FOXP3 protein as a specific biomarker (stained with IHC) in digitalized breast cancer samples.

1.1 Tissue samples and digitization

The FOXP3 protein was stained using IHC, then a primary antibody against this protein is employed to stain the tissue samples, followed by staining with 3,3´-diaminobenzidine (DAB) and counterstaining with hematoxylin (H). Im-

* PhD advisors: Prof. Carlos Pablo Lopez and Prof. Marylène Marie Leyene

ages of tissues show brown nuclei among blue ones, where the former are regulatory T lymphocytes and the latter the other cells.

Digital images of breast tissue samples were obtained by scanning the slides with the PANNORAMIC 250 Flash 3D Histech scanner.

We use five images from the available digitally scanned images batch, which differ substantially in shape and structure.

1.2 Baseline procedure

The Oncological Pathology & Bioinformatics research group of *IISPV* made the baseline technique for FOXP3 nuclei (stained with IHC) automatic edge detections and tissue area recognition (counter stained with hematoxylin) in the slides using the Fiji program as previously described in [3].

The baseline is a ruled-based technique in which first they detect for each given image the tissue region and then the FOXP3 nuclei inside of it.

Thus, there are two main subphases, each consisting of a preprocessing phase, segmentation mask creation, postprocessing phase, and edge detection.

First, we port the baseline procedure to Python to facilitate the task automation of edge detections. Moreover, Python now has a larger community than in Fiji and is more flexible.

The preprocessed image of the two subphases is a one-channel image, from which is made the segmentation mask, followed by a postprocessing phase for decreasing the noise quantity in the edge detection. Regarding the tissue area segmentation mask creation porting, we remark that we have done a bit different job concerning the baseline procedure since by detecting the fat areas in the tissue slide, we do not consider them as part of the tissue.

By doing that, we do not assume as part of the tissue slide area where there are no nuclei.

2 Methodology

Because the threshold used to create the segmentation mask from the one-channel image is hand chosen and is the same for all the images to be segmented, we try image processing techniques that work on the threshold.

Then, in the postprocessing phase, we integrate an image-processing technique called morphological opening to see if we can remove noise from the FOXP3 nuclei segmentation mask image or if we lose too much information. The aim of applying morphological opening on nuclei edge detections is to reduce the number of false positives. As a result, we conduct an ablation study to assess the contribution of morphological opening to the edge detection task with the new threshold proposals and on the baseline procedure. The newly introduced thresholds are otsu, triangle method, mean method, adaptive thresholding, and adaptive gaussian thresholding.

Following that, we use two Artificial Intelligence techniques: K-means, an unsupervised Machine Learning algorithm, and a neural network called UNet, previously pre-trained for nuclei segmentation. The first is used for both edge detections, whereas UNet is exploited only for FOXP3 nuclei detection. We use UNet to segment FOXP3 directly from the original images to see if we can skip the preprocessing phase using this novel Deep Learning technique.

Because UNet produces a grey-scale segmentation mask, we use the otsu threshold (O) or K-means (K) to generate the final segmentation mask. Furthermore, because the UNet requires a three-channel image as input, we use the preprocessed image for all three channels (1) or the original image (2).

If some of these techniques have bad performances for tissue edge detection, FOXP3 nuclei edge detection, or both, we do not show the performances of some of them in the next section. Thus, we do show only the relevant results of specific selected techniques.

To quantify the performance of slide and nuclei segmentation, we conduct an ablation study and use the baseline procedure without applying morphological opening as the ground truth.

We evaluate segmentation mask creation performances using several metrics, including the Jaccard index, Dice coefficient score, which is equivalent to the F1 score in this case study, recall, precision, and the area under the precision-recall curve, called average precision. In Table 2 appears the *Ratio* metric, which is the percentage of nuclei pixels quantified for each image processing method divided by the pixel tissues identified by the baseline procedure.

3 Results

In tissue slide edge detection, we recognize that the triangle method achieves nearly the same results as the baseline procedure. Following an analysis phase, we discovered that the first image is the most difficult for edge detection. Indeed, after postprocessing the K-means segmentation mask, we found that the tissue is not detected. We will not show the performances with and without considering the first image for adaptive thresholding and adaptive gaussian thresholding since they have bad performances. After that, since for the case without considering the first image we want to show the improvement of the performances of K-means, we will not show also for this case the otsu thresholding and the mean method.

If we analyse Table 1, we can see that the performances improve if we do not evaluate the first image. By doing that, K-means has the best precision score, with the same performance of the baseline technique.

We can view in Table 2 the relevant results selected from the ablation study for FOXP3 nuclei edge detection mean performances. As we can note, we do not show triangle method, adaptive thresholding and adaptive gaussian

Images	*Technique*	*Jaccard index*	*Average precision*	*F1 score*	*Recall*	*Precision*
All images	K-means	0.5762	0.6446	0.6646	0.5762	0.8000
	Mean	0.4296	0.4298	0.5799	0.9936	0.4314
	Otsu	0.4122	0.4084	0.5591	0.8799	0.4254
	Triangle	**0.9655**	**0.9655**	**0.9822**	**1.0000**	**0.9655**
No Image 1	K-means	0.7202	0.7816	0.8307	0.7202	**1.0000**
	Triangle	**0.9728**	**0.9728**	**0.9860**	**1.0000**	0.9728

Table 1. Relevant results of tissue edge detection mean performances with and without taking into consideration Image 1 extracted from the ablation study

thresholding since they have low performances. Then, we show for the UNet only the variant with the input of the original image and the otsu thresholding application.

Table 1 does not depict the results of the other three UNet variants since they have low performances.

Technique	*Morph. opening*	*Jaccard index*	*Average precision*	*F1 score*	*Recall*	*Precision*	*Ratio*
K-means	No	0.6261	0.6262	0.7265	0.9993	0.6269	0.3853
	Yes	**0.6718**	**0.6678**	**0.7794**	0.9495	**0.6998**	0.2568
Mean	No	0.2389	0.2389	0.3820	**1.0000**	0.2389	0.9468
	Yes	0.2094	0.2094	0.3409	**1.0000**	0.2094	0.9860
Otsu	No	0.5909	0.5909	0.6983	0.9995	0.5914	0.4322
	Yes	0.5436	0.5436	0.6497	0.9997	0.5439	0.5445
UNet2O	No	0.2574	0.2160	0.4078	0.4739	0.3733	0.0795
	Yes	0.2609	0.2187	0.4122	0.4916	0.3679	**0.0898**
Baseline	No	—	—	—	—	—	0.1078

Table 2. Relevant results of FOXP3 nuclei edge detection mean performances extracted from the ablation study

As we can see in Table 2, we achieve the best overall results in positive nuclei segmentation by combining the K-means with the morphological opening. We have the best recall using the mean thresholding, so we can recognize where all the nuclei are, but this is due to many false positives, so it is better to use the K-means with the morphological opening, which has a recall of 0.9495. With respect to the *Ratio* or the percentage of nuclei pixels divided by tissue pixel slides, the UNet2O technique with the morphological opening has the most similar ratio concerning the baseline.

However, since the other performances are not quite as good, it is better to use the K-means, which has a higher *Ratio* and thus introduces some false positive pixel areas.

4 Discussion

By dividing the problem into tissue edge detection and nuclei edge detection, we can see that triangle method is better for the former and K-means is better for the latter. K-means is adequate for tissue edge detection but it is not robust, since after applying postprocessing to one of the five images, we can note that we are not able to recover its tissue boundary. We can see from UNet that we do not have pretty good results. Since the pre-trained UNet is used for nuclei segmentation, if we use the original image as input, the neural network becomes confused since there are also nuclei highlighted by hematoxylin.

5 Conclusion and Future Works

Tissue and positive nuclei automatic edge detections are thrilling challenges. We explored various approaches, using the baseline procedure as a reference, and discovered that the triangle method has the best performances for tissue edge detection and K-means for FOXP3 nuclei edge detection. Regarding the techniques derived from the UNet, we discovered their performances are not as good as the previously mentioned. However, since we used a pre-trained neural network, we should look for other variants in the future. Some prospects include exploring other neural network proposals and further preprocessing and postprocessing techniques.

Acknowledgement. This research is a starting point for the funded BosomShield project, with grant agreement ID: 101073222.

Special thanks to Oncological Pathology & Bioinformatics group of *IISPV* in Tortosa for the idealization of the baseline procedure definition.

References

[1] Burugu, Samantha and Asleh-Aburaya, Karama and Nielsen, Torsten Immune infiltrates in the breast cancer microenvironment: detection, characterization and clinical implication *Springer, Faculty Research and Publications*, May, 2016.

[2] Mastrosimini MG, Eccher A, Nottegar A et al. WSI validation studies in breast and gynecological pathology *Pathol Res Pract.*, Dec, 2022.

[3] Callau C, Lejeune M, Korzynska A, et al. Evaluation of cytokeratin-19 in breast cancer tissue samples: a comparison of automatic and manual evaluations of scanned tissue microarray cylinders. *Biomed Eng Online*, 14 Suppl 2(Suppl 2):S2, Aug 13, 2015.

Graph Generative Models for Regression Tasks

Sarah A. Fadlallah *

Department of Computer Engineering and Mathematics, Universitat Rovira i Virgili
Tarragona, Spain
sarah.fadlallah@urv.cat

Problem Statement

Graphs are a powerful tool for understanding complex data structures and their attributes. However, representing a graph and its node attributes as a vector, known as graph embedding, can be challenging. Traditional statistical methods for graph embedding can be time and resource-intensive. Graph Autoencoders (GAEs) have emerged as a promising alternative for reconstructing or generating new graphs with similar features [1].

While neural networks have made significant progress in addressing various problems, there are limited applications of graph regression, especially in the case of Semi-Supervised Learning (SSL) [3].

Objective

To effectively learn hidden patterns in graphs, it is important to distinguish between node-dependent semantic knowledge and edge-dependent structural knowledge. By separating these features, the impact of specific attributes on the model's performance can be analysed [2, 5].

Our objective is to leverage GAEs and similar techniques to identify the optimal feature set for graph embedding, with applications in prediction and generative models, specifically in the realm of pharmaceutical drug discovery.

Methodology

Our goal is to improve predictions of a graph's global property, drug potency in this case, by using an autoencoder and a GAE to extract both semantic and structural features from a given graph. The GAE's encoder component creates a latent matrix $\boldsymbol{Z} \in \mathbb{R}^{\boldsymbol{n} \times \boldsymbol{b}}$ using graph structural features such as

* PhD advisor: Francesc Serratosa, Carme Julià

atomic position, while the decoder reconstructs the adjacency matrix. In contrast, the autoencoder generates a latent matrix using semantic features only. The learning algorithm minimises the difference between the original and reconstructed adjacency matrices. The proposed method is illustrated in Figure 1.

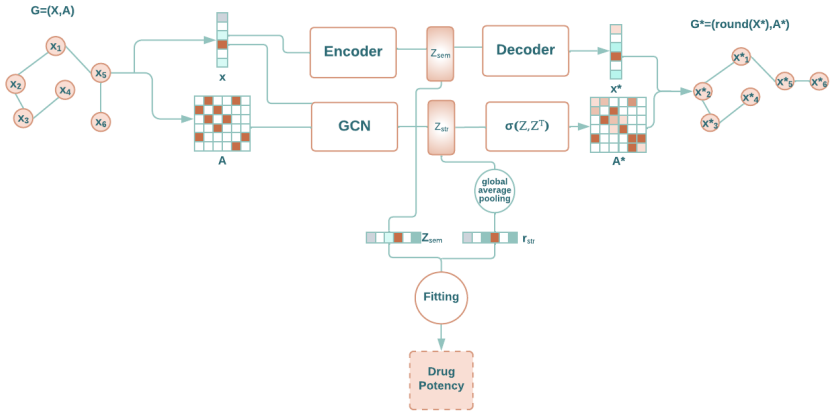

Fig. 1. An illustration of our architecture for performing graph regression based on an autoencoder and a graph autoencoder

The encoder's function of GCN can be expressed as Equation 1 :

$$\boldsymbol{Z} = GCN(\boldsymbol{X}, \boldsymbol{A}) = \tilde{\boldsymbol{A}} ReLU\left(\tilde{\boldsymbol{A}}\boldsymbol{X}\boldsymbol{W_0'}\right)\boldsymbol{W_1'} \tag{1}$$

where $\tilde{\boldsymbol{A}}$ is a symmetrically normalised adjacency matrix computed from $\boldsymbol{A}$, while $\boldsymbol{W_0'}$ and $\boldsymbol{W_1'}$ are the weight matrices of each layer.

The decoder is defined as Equation 2:

$$\boldsymbol{A^*} = \sigma\left(\boldsymbol{Z}\boldsymbol{Z^T}\right) \tag{2}$$

where $\boldsymbol{\sigma}(\cdot)$ is the sigmoid function, $\boldsymbol{T}$ means the transposed matrix. The output $\boldsymbol{A^*}$ represents edge probabilities in the reconstructed matrix. The learning algorithm minimises the mean square distance between matrices. The resulting vectors are then used for the global property prediction

Preliminary results and future directions

The results indicate that the selection of attributes that are included or excluded from a graph has a noticeable impact on the representation of the graph and, consequently, the quality of the predictions. These findings suggest that creating a dual model that utilises this attribute selection approach could lead to improved predictions. Plots in Figure 2 show a comparison of the Mean Square Errors(MSE) of regression performed on latent vectors capturing different attributes with different architectures.

Future work will include defining a model that can create vectors that are valid for better graph regeneration as well as regression.

Acknowledgement. This research is supported by the Martí Franquès program in addition to AGAUR research group 2021SGR-00111: "ASCLEPIUS: Smart Technology for Smart Healthcare".

References

[1] Kipf, T. N. and Welling, M. Semi-Supervised Classification with Graph Convolutional Networks. *CoRR*, abs/1609.02907, 2016.

[2] Kipf, T. N., Fetaya, E., Wang, K., Welling, M., and Zemel, R. Neural Relational Inference for Interacting Systems. In International Conference on Machine Learning, 2018.

[3] Kostopoulos, Georgios and Karlos, Stamatis and Kotsiantis, Sotiris and Ragos, Omiros. Semi-supervised regression: A recent review. *Journal of Intelligent & Fuzzy Systems*, 35:1-18, June 2018. doi: 10.3233/JIFS-169689.

[4] Le, T., Le, N., and Le, B. Knowledge graph embedding by relational rotation and complex convolution for link prediction. *Expert Systems with Applications*, 214:119122, March 15 2023. doi: 10.1016/j.eswa.2022.119122. ISSN: 0957-4174, EISSN: 1873-6793.

[5] Zhang, M., Cui, Z., Neumann, M., and Chen, Y. An End-to-End Deep Learning Architecture for Graph Classification. In Proceedings of the AAAI Conference on Artificial Intelligence, 2018.

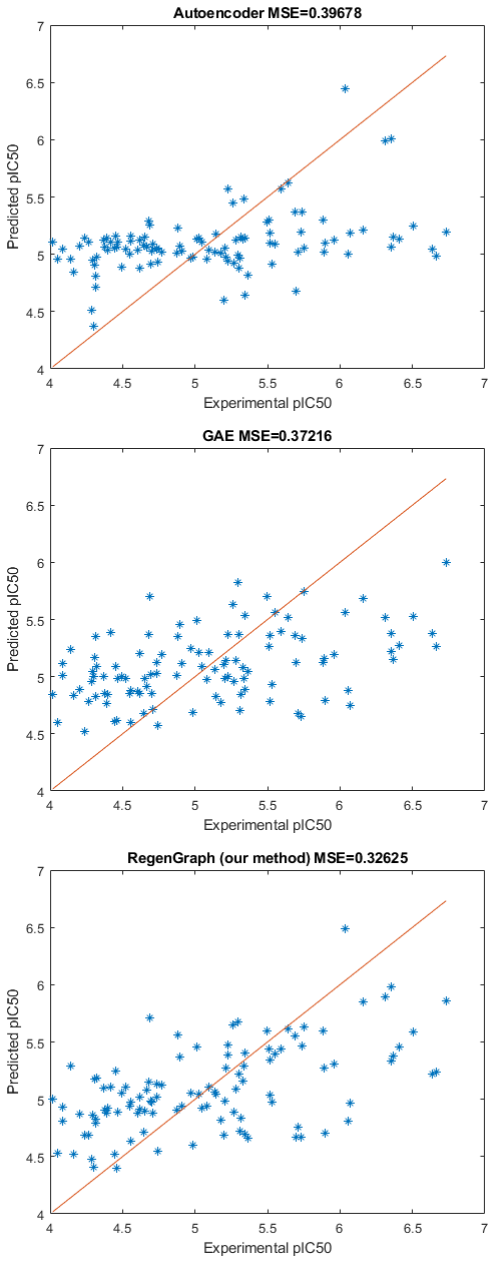

Fig. 2. Scatter plots compare predicted vs. experimental pIC_{50} values for compounds using Autoencoder-only, GAE-only, and our combined model, with MSE shown on top.

Deep learning radiomics for breast tumor malignancy prediction in ultrasound images

Mohamed A.Hassanien *

Department of Computer Engineering and Mathematics, Universitat Rovira i Virgili Tarragona, Spain
mohamed.abdelhameedhassanien@estudiants.urv.cat

1 Introduction

According to WHO (World Health Organization) reports, breast cancer is one of the most common cancers in women worldwide. The malignant growth of BC begins within the duct or lobule, where it usually does not cause symptoms and has a low risk of extending to other body parts (i.e., metastasis). In situ breast tumors can grow and intrude into surrounding breast tissue, then spread to nearby lymph nodes or other organs (i.e., distant metastasis). It is worth noting that widespread metastasis is the leading cause of death in breast cancer patients [1]. The presently used clinical breast imaging modalities are mammography, magnetic resonance imaging (MRI), and ultrasound imaging (US). Currently, MRI and US are only auxiliaries to mammography. Mammography imaging sensitivity is approximately 75%, which can be dropped to 50% in young women whose breast tissues frequently have a higher breast density. Hence, the use of mammography and US imaging could significantly enhance the sensitivity of the test for the diagnosis of such cases [2]. Unlike other imaging modalities such as MRI, breast ultrasound (BUS) technology is very cheaper, fast, and easily accessible to people in a community. BUS imaging offers scanning feasibility to women who are at high risk of breast cancer disease.

2 Methods and Materials

Figure 1 presents an overview of the proposed approach for predicting breast cancer malignancy from BUS images. As shown, the proposed method comprises three main components: 1) an emerging deep learning network so-called ConvNeXt [3] to extract robust radiomics, 2) a pooling mechanism to generate the malignancy score of each input BUS sequence, and 3) a visual explanation algorithm to help interpret deep learning decisions.

* PhD advisor: Mohamed Abdelnasser and Domenec Puig

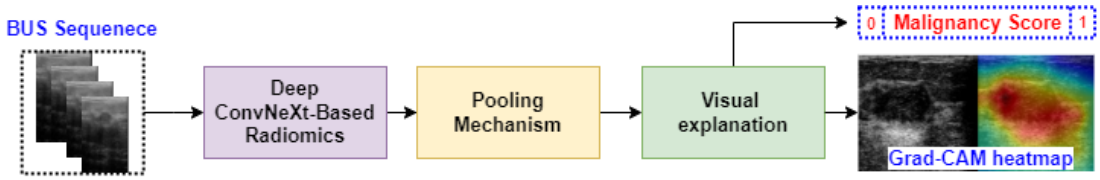

Fig. 1. Overview of deep ConvNeXt-based radiomics for breast tumor malignancy prediction from BUS sequences.

2.1 Deep ConvNeXt-based radiomics

Here, we employ ConvNeXt [3] to extract robust radiomics to classify breast cancer tumors as benign or malignant. In ConvNeXt, the architecture of the standard CNNs is modernized to the construction of a hierarchical vision Transformer. As discussed in [3], the starting point of ConvNeXt is a ResNet-50 [4] model, which has four stages, each contains several blocks. In ConvNeXt, the ResNet-50 model has been trained with similar training techniques used to train vision Transformers.

2.2 Malignancy score pooling mechanism

In this work, we propose to classify benign and malignant breast tumors based on BUS sequences instead of single BUS images. In particular, we extract radiomics based on ConvNeXt from each frame in the BUS sequence and estimate the malignancy score of each frame. We calculate the malignancy score of the whole input BUS sequence as follows:

$$S_M = \frac{1}{N_q} \sum w_i s_i \tag{1}$$

where s_i is the malignancy score of frame i, $W = [w_1, w_2, \ldots, w_N]$ is a weighting vector with a length N, where any element w_i may hold 0 or 1. An element in W will have a value of 1 if the quality of the BUS frame exceed the thresholds of the brightness and blurriness scores, and N_q is the number of the frames in the BUS sequence exceeding the thresholds of the brightness and blurriness scores.

2.3 Visual explanation and interpretation

This paper employs different techniques to produce visual explanations for the proposed ConvNeXt-based radiomics system's decisions to make it explainable. Specifically, we utilize the Grad-CAM method (i.e., Gradient-weighted Class Activation Mapping) and present the overall malignancy score overlaid on the BUS images. The Grad-CAM technique employs the gradients of any target class, e.g., malignant tumor in our ConvNeXt-based radiomics network,

streaming into the last Conv layer to create a localization map emphasizing the vital regions in the input image that participate in the prediction of the class [5].

2.4 Evaluation metrics

In this study, the performance of the proposed approach has been assessed using different evaluation metrics, namely accuracy, precision, recall, and F1-score. These metrics can be defined as follows [6]:

$$\text{Accuracy} = \frac{TP + TN}{P + N} \tag{2}$$

$$\text{Precision} = \frac{TP}{TP + FP} \tag{3}$$

$$\text{Recall} = \frac{TP}{TP + FN} \tag{4}$$

$$\text{F1-score} = \frac{TP}{TP + \frac{1}{2}(FP + FN)} \tag{5}$$

In these expressions, TP stands for the number of malignant BUS sequences correctly classified as malignant; TN stands for the number of benign BUS sequences correctly classified as benign; FP stands for the number of benign BUS sequences wrongly classified as malignant; FN stands for the number of malignant BUS sequences wrongly classified as benign.

2.5 Dataset

A database of 31 malignant and 28 benign BUS sequences is used to build and evaluate the proposed CAD system, where each BUS sequence corresponds to a patient. This dataset is part of a clinical database of ultrasonic radio-frequency strain imaging data created by the Engineering Department of Cambridge University.The number of ultrasound images in the benign and malignant BUS sequences is 3911 and 5245, respectively.

3 Experimental Results

Table 1 presents the performance of different deep CNN-based radiomics extracted from a single BUS image to differentiate between benign and malignant tumors. Specifically, we employ EfficientNetV2 [7], EfficientNet-B7 [8], MobileNetV3 [9], and ResNet-101 [4] to classify breast tumors as benign or malignant. As one can see in Table 1, MobileNetV3-based radiomics outperforms EfficientNetV2, EfficientNet-B7 and ResNet-101. It achieves an accuracy of 88.17%, precision of 88.60%, recall of 86.60%, and F1-score of 87.28% [10].

EfficientNetV2- and EfficientNet-B7 -based radiomics obtains similar results with an accuracy lower than 85%. ResNet-101 achieves the second-best classification results, where it obtains an accuracy rate $2-3\%$ higher than EfficientNetV2 and EfficientNet-B7 -based radiomics. The F1-score of MobileNetV3 is 3% higher than ResNet-101. The breast tumor classification results of different vision transformer-based radiomics extracted from a single BUS image. Here, vision transformer (ViT) [11], ResMLP [12], Swin Transformer [13], and ConvNeXt [3] are employed. ConvNeXt outperforms all other transformers in classifying breast tumors with accuracy, precision, recall, and F1-score higher than 88%.

Table 1. Results of SUI BUS CAD systems based on different CNN networks. The best results are highlighted in bolds.

2*Model	**Metrics**			
	Accuracy (%)	Precision (%)	Recall (%)	F1-score (%)
EfficientNetV2 [7]	83.09	85.31	79.70	81.04
EfficientNet-B7 [8]	82.30	85.94	78.24	79.71
MobileNetV3 [9]	**88.17**	**88.60**	**86.48**	**87.28**
ResNet-101 [7]	85.20	84.81	83.98	84.31

4 Conclusions

This work proposed an efficient deep learning-based radiomics method for predicting breast cancer malignancy from BUS sequences. The proposed method consists of three main a deep ConvNeXt network to extract robust radiomics to predict the malignancy score of breast tumors, 2) a pooling mechanism to generate the malignancy score of each input BUS sequence, and 3) a visual explanation step to generate heat maps superimposed on ultrasound images. A BUS sequence dataset containing 31 malignant and 28 benign cases was used to assess the efficacy of the proposed method. The proposed method achieved accuracy and F1-score higher than 91%. Besides, the F1-score of the proposed approach was 4% higher than the single ultrasound image CAD system based on ConvNeXt.

Acknowledgement. The Spanish Government partly supported this research through project PID2019-105789RB-I00.

References

[1] Gurdeep S Mannu, Zhe Wang, John Broggio, Jackie Charman, Shan Cheung, Olive Kearins, David Dodwell, and Sarah C Darby. Invasive breast cancer and

breast cancer mortality after ductal carcinoma in situ in women attending for breast screening in england, 1988-2014: population based observational cohort study. *Bmj*, 369, 2020.

[2] Sepideh Iranmakani, Tohid Mortezazadeh, Fakhrossadat Sajadian, Mona Fazel Ghaziani, Ali Ghafari, Davood Khezerloo, and Ahmed Eleojo Musa. A review of various modalities in breast imaging: technical aspects and clinical outcomes. *Egyptian Journal of Radiology and Nuclear Medicine*, 51(1):1–22, 2020.

[3] Zhuang Liu, Hanzi Mao, Chao-Yuan Wu, Christoph Feichtenhofer, Trevor Darrell, and Saining Xie. A convnet for the 2020s. *arXiv preprint arXiv:2201.03545*, 2022.

[4] Kaiming He, Xiangyu Zhang, Shaoqing Ren, and Jian Sun. Deep residual learning for image recognition. In *Proceedings of the IEEE conference on computer vision and pattern recognition*, pages 770–778, 2016.

[5] Ramprasaath R Selvaraju, Michael Cogswell, Abhishek Das, Ramakrishna Vedantam, Devi Parikh, and Dhruv Batra. Grad-cam: Visual explanations from deep networks via gradient-based localization. In *Proceedings of the IEEE international conference on computer vision*, pages 618–626, 2017.

[6] Bradley J Erickson and Felipe Kitamura. Magician's corner: 9. performance metrics for machine learning models, 2021.

[7] Mingxing Tan and Quoc Le. Efficientnetv2: Smaller models and faster training. In *International Conference on Machine Learning*, pages 10096–10106. PMLR, 2021.

[8] Mingxing Tan and Quoc Le. Efficientnet: Rethinking model scaling for convolutional neural networks. In *International conference on machine learning*, pages 6105–6114. PMLR, 2019.

[9] Brett Koonce. Mobilenetv3. In *Convolutional Neural Networks with Swift for Tensorflow*, pages 125–144. Springer, 2021.

[10] Vivek Singh Mohamed A.Hassanien Mohamed Abdel-Nasser, Domenec Puig. Predicting breast tumor malignancy using deep convnext radiomics and quality-based score pooling in ultrasound sequences. *Diagnostics*, 12, 2022.

[11] Alexey Dosovitskiy, Lucas Beyer, Alexander Kolesnikov, Dirk Weissenborn, Xiaohua Zhai, Thomas Unterthiner, Mostafa Dehghani, Matthias Minderer, Georg Heigold, Sylvain Gelly, et al. An image is worth 16x16 words: Transformers for image recognition at scale. *arXiv preprint arXiv:2010.11929*, 2020.

[12] Hugo Touvron, Piotr Bojanowski, Mathilde Caron, Matthieu Cord, Alaaeldin El-Nouby, Edouard Grave, Gautier Izacard, Armand Joulin, Gabriel Synnaeve, Jakob Verbeek, et al. Resmlp: Feedforward networks for image classification with data-efficient training. *arXiv preprint arXiv:2105.03404*, 2021.

[13] Ze Liu, Yutong Lin, Yue Cao, Han Hu, Yixuan Wei, Zheng Zhang, Stephen Lin, and Baining Guo. Swin transformer: Hierarchical vision transformer using shifted windows. In *Proceedings of the IEEE/CVF International Conference on Computer Vision*, pages 10012–10022, 2021.

Roudneff's Conjecture in dimension 4

Rangel Hernández Ortiz *

Department of Computer Engineering and Mathematics, Universitat Rovira i Virgili
Tarragona, Spain
rangel.hernandez@urv.cat

Abstract. J.-P. Roudneff conjectured in 1991 that every arrangement of $n \geq 2d+1 \geq 5$ (pseudo) hyperplanes in the real projective space $\mathbb{P}^d$ has at most $\sum_{i=0}^{d-2} \binom{n-1}{i}$ cells bounded by each hyperplane. The conjecture is true for $d = 2, 3$. The main result of this manuscript, is to show the validity of this conjecture for $d = 4$.

Keywords: Roudneff's conjecture, Oriented Matroids, Arrangements of Hyperplanes.

1 Introduction

An *Euclidean* (resp. *projective*) d-arrangement of n hyperplanes $H(d, n)$ is a finite collection of hyperplanes in the Euclidean space $\mathbb{R}^d$ (resp. the real projective space $\mathbb{P}^d$) such that no point belongs to every hyperplane of $H(d, n)$. Any arrangement $H(d, n)$ decomposes $\mathbb{R}^d$ (resp. $\mathbb{P}^d$) into a d-dimensional cell complex. It is clear that any d-cell c of $H(d, n)$ has at most n *facets* (that is, $(d-1)$-cells). We say that c is a *complete cell* of $H(d, n)$ if c has exactly n facets, i.e., c is bounded by each hyperplane of $H(d, n)$.

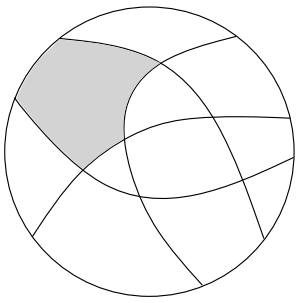

Fig. 1. An arrangement of 5 hyperplanes in $\mathbb{P}^2$. The gray cell is a complete cell.

* PhD advisor: Luis Pedro Montejano

The *cyclic polytope* of dimension d with n vertices, discovered by Carathéodory [2], is the convex hull in $\mathbb{R}^d$ of $n \geq d+1 \geq 3$ different points $x(t_1), \ldots, x(t_n)$ of the moment curve $x : \mathbb{R} \longrightarrow \mathbb{R}^d,\ t \mapsto (t, t^2, \ldots, t^d)$. Cyclic polytopes play an important role in the combinatorial convex geometry due to their connection with certain extremal problems, For example, the Upper Bound theorem due to McMullen [8]. *Cyclic arrangements* are defined as the dual of the cyclic polytopes. As for cyclic polytopes, cyclic arrangements also have extremal properties. For instance, Shannon [9] has introduced cyclic arrangements on dimension d as examples of projective arrangements with a minimum number of cells with $(d+1)$ facets.

Let denote by $C_d(n)$ the number of complete cells of the cyclic arrangements on dimension d with n hyperplanes. Roudneff [6] proved that $C_d(n) \geq \sum_{i=0}^{d-2} \binom{n-1}{i}$ and that is tight for all $n \geq 2d+1$. Moreover, he conjectured that in that case, cyclic arrangements have the maximum number of complete cells.

Conjecture 1. [6, Conjecture 2.2] Every arrangement of $n \geq 2d+1 \geq 5$ (pseudo) hyperplanes in $\mathbb{P}^d$ has at most $C_d(n)$ complete cells.

The conjecture is true for $d = 2$ (that is, any arrangement of n pseudolines in $\mathbb{P}^2$ contains at most one complete cell), Ramírez Alfonsín [5] proved the case $d = 3$ and in [7] the authors proved it for arrangements arising from Lawrence oriented matroids.

In [3] calculated the exact number of complete cells of cyclic arrangements for any positive integers d and n with $n \geq d+1$, namely,

$$C_d(n) = \binom{d}{n-d} + \binom{d-1}{n-d-1} + \sum_{i=0}^{d-2} \binom{n-1}{i}. \tag{1}$$

Thus, in view of Roudneff's conjecture, Montejano and Ramírez Alfonsín [7] asked the following.

Question 1. Is it true that every (pseudo) arrangement of $n \geq d+1 \geq 3$ hyperplanes in $\mathbb{P}^d$ has at most $C_d(n)$ complete cells?

The main result of this work is to answer affirmatively to Question 1 for $d = 4$. As a consequence, we prove Roudneff's conjecture for dimension 4, giving more credit to the general conjecture. Moreover, with some simple observations, we can finish answering to Question 1 for $d = 3$.

2 Oriented matroids

Let us briefly give some basic notions and definitions on oriented matroid theory. We refer the reader to [1] for background on oriented matroid theory.

A *signed set* or *signed vector* X is a set $\underline{X}$ together with a partition (X^+, X^-) of $\underline{X}$ into two distinguished subsets: X^+, the set of *positive elements* of X, and X^-, its set of *negative elements*. The set $\underline{X} = X^+ \cup X^-$ is the *support* of X.

An oriented matroid M on a finite set E is defined by its collection $\mathcal{C}$ of some signed sets, called circuits, satisfying certain properties. A *positive circuit* X is a circuit with $X^- = \emptyset$. We say that the matroid $M = (E, \mathcal{C})$ is *acyclic* if it does not contain positive circuits (otherwise, M is called *cyclic*). A *reorientation* of M on $R \subseteq E$ is performed by changing the signs of the elements in R in all the circuits of M. It is easy to check that the new set of signed circuits is also the set of circuits of an oriented matroid, usually denoted by ${}_{-R}M$. A reorientation is *acyclic* if ${}_{-R}M$ is acyclic. Recall that a rank r oriented matroid on n elements is *uniform* if its set of circuits consists of all $r+1$-element subsets of $[n]$.

Given two sign-vectors $X, Y \in \{+1, -1, 0\}^E$ (we will abbreviate it by $X, Y \in \{+, -, 0\}^E$), their *separation* is the set $S(X, Y) = \{e \in E \mid X_e \cdot Y_e = -\}$, where X_e and Y_e are the sings of the element e in $\underline{X}$ and $\underline{Y}$, respectively. For convenience, we denote by $H(X, Y) = \{e \in E \mid X_e \cdot Y_e = +\}$. We say that X and Y are *orthogonal* if the sets $S(X, Y)$ and $H(X, T)$ are either both empty or both non-empty. Let us define

$$X \perp Y = \min\{|H(X, T)|, |S(X, T)|\}.$$

Maximal covectors of an oriented matroid $M = (E, \mathcal{C})$ are usually called *topes*. Thus, notice that a tope T is a sign vector $T \in \{+, -\}^E$ and a circuit X is a sign vector $X \in \{+, -, 0\}^E$ with $|\underline{X}| > 0$. Then, X and T are *orthogonal* if $X \perp T \geq 1$. It is known that a tope is a sign vector $T \in \{+, -\}^E$ such that $T \perp X \geq 1$ for all circuit $X \in \mathcal{C}$.

3 Topological Representation Theorem

Many of the combinatorial properties of arrangements of (pseudo) hyperplanes can be studied in the language of oriented matroids. The so-called Topological Representation Theorem, due to Folkman and Lawrence [4], states that the acyclic reorientation classes of oriented matroids on n elements and rank r (without loops or parallel elements) are in one-to-one correspondence with the classes of isomorphism of arrangements of n (pseudo) hyperplanes in $\mathbb{P}^{r-1}$.

An arrangement $H(d, n)$ is called *simple* if $n \geq d$ and every intersection of d pseudo-hyperplanes is a unique distinct point. It is known that simple arrangements correspond to uniform oriented matroids. The d-cells of any arrangement $H(d, n)$ are usually called topes since they are in one-to-one correspondence with the topes of the oriented matroids M on n elements of rank $r = d + 1$ of its corresponding acyclic reorientation class. It is known

that a tope is a complete cell if reorienting any single element, the resulting sign-vector is also a tope.

4 Main results

Theorem 1. *Each of the* 135 *acyclic reorientation classes of uniform rank* 5 *oriented matroids on* 8 *elements have at most* $C_4(8)$ *complete cells. Moreover, there is only* 1 *acyclic reorientation class with exactly* $C_4(8)$ *complete cells.*

Theorem 2. *Each of the* 9 276 595 *acyclic reorientation classes of uniform rank* 5 *oriented matroids on* 9 *elements have at most* $C_4(9)$ *complete cells. Moreover, the class of the alternating oriented matroid is the only one with exactly* $C_4(9)$ *complete cells.*

Theorem 3. *Every arrangement of* $n \geq 5$ *(pseudo) hyperplanes in* $\mathbb{P}^4$ *has at most* $C_4(n)$ *complete cells.*

Acknowledgement. Thanks to Martí i Franquès programme for the provided grant.

References

[1] B. Björner, M. Las Vergnas, B. Sturmfels, and N. White, G. Ziegler. Oriented Matroids. *2 ed., Encyclopedia of Mathematics and its Applications*, 1999.

[2] C. Carathéodory. Über den Variabilitätsbereich des Koeffizienten von Potentzreihen die gegberne Wette nicht annehmen. *Math. Ann.*, 64:95–115, 1904.

[3] D. Forge and J. L. Ramírez Alfonsín. On counting the k-face cells of cyclic arrangements. *Europ. J. Combinatorics*, 22:307–312, 2001.

[4] J. Folkman and J. Lawrence. Oriented matroids. *J. Comb. Theory Ser. B*, 25:199–236, 1978.

[5] J. L. Ramírez Alfonsín. Cyclic arrangements and Roudneff's conjecture in the space. *Inform. Process. Lett.*, 71:179–182, 1999.

[6] J.-P. Roudneff. Cells with many facets in arrangements of hyperplanes. *Discrete Math.*, 98:185–191, 1991.

[7] L.P. Montejano and J. L. Ramírez Alfonsín. Roudneffs Conjecture for Lawrence Oriented Matroids. *Electronic Journal of Combinatorics*, 22(2), P2-3, 1-14, 2015.

[8] P. McMullen. The maximal number of faces of a convex polytope. *Mathematika*, 17:179–184, 1970.

[9] R.W. Shannon. Simplicial cells in arrangements of hyperplanes. *Geom. Dedicata*, 8:179–187, 1979.

The effect of group interactions on contagion processes

Giulio Burgio *

Department of Computer Engineering and Mathematics, Universitat Rovira i Virgili
Tarragona, Spain
giulio.burgio@urv.cat

Abstract. Contagion processes have been proven to fundamentally depend on the structural properties of the interaction networks conveying them. Such networks, understood as graphs of pairwise relations (edges), are however unsuitable to describe higher-order, group interactions involving many units at a time. Such interactions cannot be reduced to combinations of pairwise ones and therefore call for higher-order representations. We summarize here our contributions to the modelling and methodological problems posed by contagion processes in higher-order networks.

1 Introduction

Epidemics, rumor spreading, behavioral adoption, and opinion dynamics are all well-known manifestations of contagion processes. By representing the set of interactions as a graph of vertices and edges, researchers have been able to gain essential understanding on how the structural properties of the interaction network affect the spreading dynamics. Graphs, however, as sets of pairwise relations (edges) cannot correctly describe higher-order, group interactions. Complex contagion processes, in which the probability of transmission is a nonlinear function of the number of contagious contacts, provide a notable example [7]. Hypergraphs, a generalization of graphs where vertices can be grouped in relations of arbitrary size (hyperedges), provide the appropriate representation for higher-order interactions (see Fig. 1).

The general objective of the thesis project is thus the proposal of physical models and theoretical methods to describe the dynamics of complex systems presenting higher-order interactions. Given a dynamical process, we aim at characterizing how the group organization of the local interactions affects the macroscopic properties of the system.

* PhD advisors: Alex Arenas, Sergio Gómez

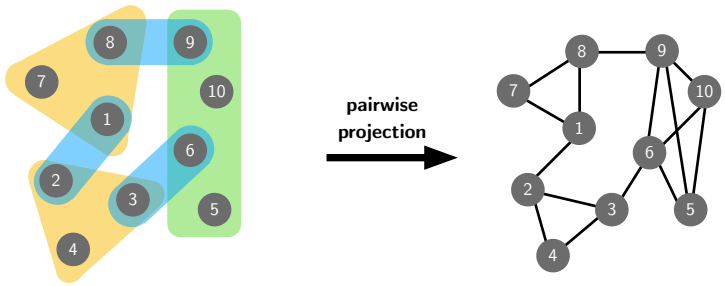

Fig. 1. Example of a hypergraph and its pairwise projection. Each colored shape indicates a hyperedge, representing the group interaction among the vertices therein. In the projection, every hyperedge is transformed in a clique of edges and the higher-order information is consequently lost.

2 Results

2.1 Complex contagions

Behaviors, strategies, conventions often require some form of social reinforcement for their adoption [7]. Repeated exposures to the same contagious source (e.g., a person with a given behavior) are usually not sufficient for the adoption to be transmitted. Instead, (simultaneous) exposure to multiple sources is needed. In order to account for this, beside a pairwise transmission probability $\beta^{(2)}$ from a contagious individual to a susceptible one, more generally, one can consider a higher-order n-wise probability of transmission $\beta^{(n)}$ coming from $n-1$ contagious individuals in a group.

Representing the set of all the interactions as a simplicial complex (a hypergraph where the existence of a hyperedge implies the existence of all its sub-hyperedges), we have been able to (i) extend to quenched structures the properties of the phase space (switch from a continuous to a discontinuous phase transition for high enough higher-order transmission rates and consequent existence of hysteresis cycles) predicted by simpler mean-field descriptions, and (ii) derive a general formula for the computation of the critical point (where the contagion-free state becomes unstable) in any simplicial complex [3]. Accounting for the dynamical correlations within any group (hyperedge), we showed –for the first time– that the critical point *does* depend on the higher-order transmission rates, proving wrong models that, neglecting those correlations, claims the contrary [1]. A new work where we derive a closed-form expression for the critical point in hypergraphs with groups of size two and three is in preparation [5].

2.2 Diffusion of cooperative behavior

Many real systems are strongly characterized by collective cooperative phenomena. In behavioral terms, cooperation is the providing of a benefit to

another individual at some cost for the provider. In well-mixed populations, where all individuals can interact with each other, evolutionary game theory predicts that selfish behavior is selected against cooperation [8]. Therefore, in order to explain the cooperation we observe, many mechanisms have been proposed, among which 'network reciprocity'. According to the latter, the mutual cooperative behavior is sustained by the existence of a network (understood as a graph) mediating either repeated strategic interactions and behavioral diffusion (e.g., via strategic imitation) among the individuals.

Through a parameterization of the structure allowing to interpolate between a graph and a hypergraph, we extended the existence of network reciprocity to group interactions [6]. Most importantly, we predicted that replacing cliques of pairwise interactions with group interactions (e.g., a cycle made of three edges with a single hyperedge of three vertices) helps cooperation to thrive. From a co-evolutionary perspective, where the interaction structures co-evolves with the behavioral state, our result could partially explain the emergence of organized groups in social systems.

2.3 Spreading dynamics under context-dependent behavior

Even when an interaction is pairwise (e.g., disease spreading), if the behavior of the involved units may be modified by the co-presence of other units (e.g., other people), the interaction cannot be considered in isolation. The group as a whole defines a 'context' which alters the (direct) interactions taking place within it. In epidemic spreading, for instance, even though each transmission concerns only two people, the likelihood of transmission is indirectly affected by the way contacts are organized within groups, for the adoption of prophylactic behaviors like face-mask wearing and physical distancing depends on the level of adoption an individual observes in the entire group. Adoption is thus mutable, contextual: an individual may exhibit one behavior or another depending on the present context. Current models either consider the group structure [9] or the disease-behavior coupling [2], but never both.

We fill this gap presenting a general model of context-dependent spreading [4]. We divide the population into two behavioral types, distinguished by a different propensity to adopt prophylactic behavior, and provide a mean-field theory to parameterize mixing patterns of any type-assortativity within groups of arbitrary size. By analyzing the distributions of groups size and type-composition, we uncover a rich phenomenology for the spreading dynamics. We show how changes in the contact organization can either facilitate or hinder epidemic spreading, primarily based on sociological factors, such as difficulty in inducing prophylactic behavior, and secondarily on prophylactic efficacy.

3 Conclusions and future work

Accounting for the group organization of interactions found in several real systems allows us to foresee new qualitative behaviors and improve quantitative predictions. Building on the knowledge we got so far, we are currently working towards two directions. On one hand, we are studying the interplay between individual and collective behavior/state, the latter understood in the form of an institution that modifies and is modified by the behavior/state of the individuals. On the other, we are developing a very general model of contagion dynamics where each individual can take part in several groups and can rewire away from them depending on their state. Such model will allow us to tackle currently unaddressed questions about the effect of group interactions.

Acknowledgement. G.B. acknowledges financial support from the European Union's Horizon 2020 research and innovation program under the Marie Skłodowska-Curie Grant Agreement No. 945413.

References

[1] A. Barrat, G. Ferraz de Arruda, I. Iacopini and Y. Moreno. Social contagion on higher-order structures. *Higher-Order Systems*: 329–346, 2022.

[2] J. Bedson et al. A review and agenda for integrated disease models including social and behavioural factors *Nature Human Behaviour*, 5(7): 834–846, 2021.

[3] G. Burgio, A. Arenas, S. Gómez and J.T. Matamalas. Network clique cover approximation to analyze complex contagions through group interactions. *Communications Physics*, 4(1): 111, 2021.

[4] G. Burgio, S. Gómez and A. Arenas. Spreading dynamics in networks under context-dependent behavior. arXiv:2211.00435, 2022. [submitted]

[5] G. Burgio, S. Gómez and A. Arenas. Triadic approximation for complex contagion on networks. [in preparation]

[6] G. Burgio, J.T. Matamalas, S. Gómez and A. Arenas. Evolution of cooperation in the presence of higher-order interactions: From networks to hypergraphs. *Entropy*, 22(7): 744, 2020.

[7] D. Centola and M. Macy. Complex contagions and the weakness of long ties. *American journal of Sociology*, 113(3): 702–734, 2007.

[8] C.P. Roca, J. Cuesta and A. Sánchez. Evolutionary game theory: Temporal and spatial effects beyond replicator dynamics. *Physics of Life Reviews*, 6(4): 208–249, 2009.

[9] G. St-Onge, V. Thibeault, A. Allard, Antoine, L.J. Dubé and L. Hébert-Dufresne. Social confinement and mesoscopic localization of epidemics on networks. *Physical review letters*, 126(9): 098301, 2021.

Fine-tuning Loss Function Hyperparameters for Improved Deep Learning-Based Ultrasound Breast Image Segmentation

Nadeem Issam Zaidkilani *

Department of Computer Engineering and Mathematics, Universitat Rovira i Virgili Tarragona, Spain
nadimkilani@gmail.com

1 Introduction

Breast cancer is a significant contributor to cancer-related death in women worldwide and has become a growing public health concern, with the urgent need for early detection. To aid physicians in diagnosing breast cancer through medical image analysis and interpretation, computer-aided diagnosis (CAD) systems have been developed in recent decades. Deep learning techniques, specifically convolutional neural networks (CNNs), have enabled successful lesion segmentation in breast ultrasound (BUS) images. In our research, we utilize cutting-edge deep learning-based semantic segmentation methods for breast tumor segmentation in BUS images.

2 Related Work

Significant advancements have been made in breast image analysis using deep learning techniques, which involve processing input images to identify high-level image representations, enabling classification and segmentation tasks. Various deep learning architectures have been proposed, such as UNET, GAN, ResNet, WideResNet, ConvNext, and CoAtNet. Attention modules and information extraction modules have been added to these architectures to control the importance of input features, improving segmentation accuracy. Self-attention layers [1] have been used to replace convolution layers in ResUnet. Transformer-based segmentation methods have become popular since the proposal of the Vision Transformer (ViT) model [2] with the swim transformer successfully applying a transformer to image semantic segmentation. Researchers have proposed various methods to address breast tumor segmentation, including a two-step method by Koshki et al. [3], an active contour

* PhD advisor: Dr.Miguel Angel Garcia and Dr.Domènec Puig Valls

method by Niaz et al. [4], and a deep learning algorithm by Goncalves et al. [5] that uses the learning of probability maps in the loss function as a regularization term for robust keypoint localization. These methods have shown improved performance compared to previous state-of-the-art methods.

3 Methodology

Choosing the appropriate loss function is a critical decision when training deep neural networks, as each function has its own advantages and disadvantages. Additionally, loss functions determine whether all image pixels have equal importance during training or if they are weighted differently based on the class label. This ensures that the minority class (in our case, tumorous regions) receives adequate attention relative to the majority class of healthy tissue. The objective of this study is to determine the optimal values of λ and γ for the Focal loss and the optimal values of α and β for Tversky loss in the baseline CoAtNet architecture.

1. **The Binary Focal Loss (LBF)** is an improved version of the Binary Cross-Entropy Loss (LBCE) that focuses on hard misclassified examples and compensates for class imbalance. LBCE penalizes pixels that are correctly classified with low confidence, resulting in a high loss. LBF modifies the shape of LBCE by introducing a factor that sharpens the loss function, reducing the loss slightly for pixels that are correctly classified even with low confidence, thereby focusing on the hard examples. To balance positive and negative pixels, a weighting factor λ is introduced in the weighted sum. Since there are more healthy pixels than tumorous pixels, the final sum tends to favor the correct segmentation of healthy regions, leading to false negatives. To reduce false negatives, the weighting factor λ can be increased for tumorous regions and reduced for healthy regions. This will increase the number of false positives but reduce the number of false negatives. As shown in equation (1)

$$LBF(\mathbf{P}, \mathbf{G}) = -\frac{1}{N}\sum_{i=1}^{N} \lambda g_i (1-p_i)^{\gamma} \log p_i + (1-\lambda)(1-g_i) p_i^{\gamma} \log(1-p_i), \tag{1}$$

where λ is typically the majority-class percentage, that is $\lambda = |\{g_i \in \mathbf{G} | g_i = 0\}|/N$, where $|\cdot|$ is the cardinality operator, and $\gamma > 0$ is the hyperparameter that controls the sharpness of the loss function (the larger, the sharper).

2. **The Tversky Loss** is an extension of the Dice loss that tackles the issue of class imbalance. It accomplishes this by adding hyperparameters, α and β, which weight the false positives (FP) and false negatives (FN) respectively.

$$LT(\mathbf{P}, \mathbf{G}) = 1 - \frac{TP + \zeta}{TP + \alpha FP + \beta FN + \zeta} \tag{2}$$

The Tversky Loss is an improvement on the Dice loss that addresses class imbalance by incorporating hyperparameters α and β, which weight false positives and false negatives. When β is greater than α, the training process focuses more on reducing false negatives, leading to increased losses for large values of FN. Consequently, minimizing the loss will prioritize reducing false negatives even if it leads to an increase in false positives. This approach will help to prevent the misclassification of tumorous regions as healthy tissue, even if there is an increase in healthy regions being wrongly classified as tumorous

4 Preliminary results and future work

This work used a dataset of breast cancer ultrasound images provided by the UDIAT Diagnostic Centre in Sabadell, Spain. The dataset consisted of 163 BUS images of different breast tumors, each associated with a ground-truth segmentation of the tumor. The dataset was divided into 113 training images and 50 testing images. The Adam optimizer with a learning rate of 0.0001 and a batch size of 4 was used for 20 epochs. Standard data-augmentation techniques were employed to increase the number of training images to 1400.

We study the best coefficients for the Focal and Tversky loss functions with CoAtNet being used as an encoder. For the Focal loss, we considered 5 different values of γ (0, 0.5, 1, 2, 5) and 5 different values of λ (0.5, 0.6, 0.7, 0.8, 0.9), and then run experiments with all 25 combinations of each γ and λ. Values of λ lower than 0.5 were discarded since λ must be above 0.5 to reduce the number of false negatives (undetected tumors) as discussed in Section 3. As for the Tversky loss, we assumed $\alpha = 1 - \beta$

and tested 4 values of β : 0.6, 0.7, 0.8, 0.9. Coefficient β must be above α to reduce the number of false negatives (undetected tumors) as discussed in Section 3.

In this work, we conducted experiments as shown in Figure 1 to find the best hyperparameters for the Focal and Tversky loss functions for the CoAtNet-based autoencoder using breast ultrasound images. We tested various values of λ and γ for Focal loss and α and β for Tversky loss and found that the best performance was achieved with $\lambda = 0.7$ and $\gamma = 5.0$ (Dice = 77%) for Focal loss and $\alpha = 0.4$ and $\beta = 0.6$ (Dice = 76%) for Tversky loss, in terms of Jaccard and Dice indices. we can conclude that, in general, the optimal values for the parameters of Focal and Tversky loss functions affect the resulting Dice index, which is a measure of segmentation accuracy. The highest Dice index for Focal loss is achieved when λ is 0.7 and γ is 5.0, while the lowest Dice index is obtained whenλ is 0.8 and γ is 0.5. Increasing γ places a greater emphasis on hard misclassified examples. For Tversky loss, the maximum Dice index is achieved when α is 0.4 and β is 0.6, and the worst Dice

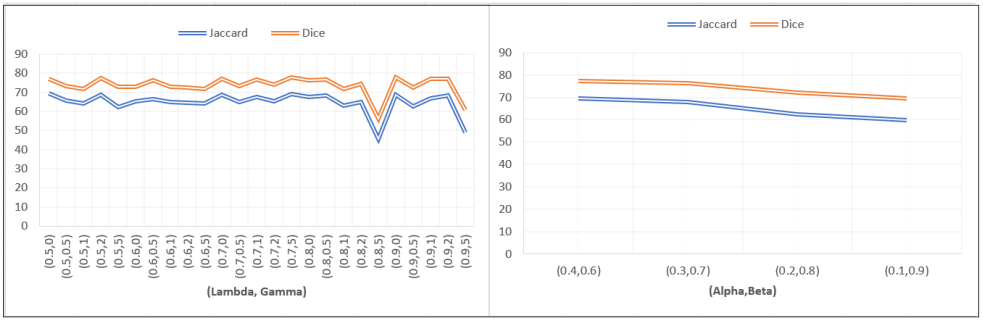

Fig. 1. Performance of Focal loss (left) and Tversky loss (right) for CoAtNet-based autoencoder

index is obtained when α is 0.1 and β is 0.9. Setting a low α value prioritizes reducing false negatives over false positives.

In future work, we will study the effects of changing the CoAtNet architecture and evaluate the effectiveness of the deep learning architecture compared to the original CoAtNet. Moreover, we will use a different dataset and other deep learning networks to compare the performance of the modified CoAtNet with other network architectures.

References

[1] Raffel C, Shazeer N, Roberts A, Lee K, Narang S, Matena M, et al. Exploring the limits of transfer learning with a unified text-to-text transformer. The Journal of Machine Learning Research. 2020;21(1):5485-551.

[2] Dosovitskiy A, Beyer L, Kolesnikov A, Weissenborn D, Zhai X, Unterthiner T, et al. An image is worth 16x16 words: Transformers for image recognition at scale. arXiv preprint arXiv:201011929. 2020.

[3] Koshki AS, Zekri M, Ahmadzadeh MR, Sadri S, Mahmoudzadeh E. Extending contour level set model for multi-class image segmentation with Application to Breast Thermography Images. Infrared Physics & Technology. 2020;105:103174.

[4] Niaz A, Memon AA, Rana K, Joshi A, Soomro S, Kang JS, et al. Inhomogeneous image segmentation using hybrid active contours model with application to breast tumor detection. IEEE Access. 2020;8:186851-61.

[5] Gonçalves T, Silva W, Cardoso MJ, Cardoso JS. Deep image segmentation for breast keypoint detection. In: Proceedings. vol. 54. MDPI; 2020. p. 35.

Domain Adaptation for Breast Cancer Classification on Mammogram Images

Mariam M. Hassan *

Department of Computer Engineering and Mathematics, Universitat Rovira i Virgili Tarragona, Spain
mariam.moustafa@urv.cat

Abstract. Breast cancer is a pervasive malignancy among women worldwide, with early detection and diagnosis being critical for successful treatment outcomes. Mammograms, which employ X-rays to visualize the internal structures of the breast, are the most effective screening and diagnostic tool for breast cancer presently available. Deep Learning has recently demonstrated remarkable success in classifying breast cancer on mammogram images. Nonetheless, deep learning's efficacy relies on two assumptions: (1) the availability of vast amounts of annotated data and (2) the sampling of training and testing data from the same distribution. Data annotation can be a daunting and expensive task, especially in the medical domain. Moreover, subtle changes in conditions or patient characteristics, such as age or ethnicity, can cause significant degradation in model performance due to a phenomenon known as domain shift. In this work, to handle these limitations, we propose novel domain adaptation techniques to improve the model generalization on distributionally shifted data without requiring label information.

1 Introduction

Breast cancer is a complex disease that requires early detection and diagnosis to ensure better patient outcomes. The high incidence and mortality rates associated with this disease have prompted extensive research into its detection and treatment. Mammograms, which are widely used as a screening tool for breast cancer, have been shown to be effective in detecting breast abnormalities, particularly in the early stages of the disease. Despite their effectiveness, mammograms are associated with certain limitations, including a high rate of false positives and false negatives, which can lead to unnecessary biopsies or missed diagnoses [1].

In recent years, deep learning-based approaches have shown great potential in improving the accuracy and reliability of mammograms. These approaches utilize large datasets of mammographic images to train deep neural networks that can accurately identify and classify breast abnormalities. However, the

* Domenec Puig, Mohamed Abdel-Nasser

performance of these models is often limited when applied to data from different sources or domains. This is due to the fact that mammographic images from different sources may have variations in imaging protocols, equipment, and patient demographics, which can affect the performance of the models [2].

Domain adaptation techniques offer a promising solution to this problem by enabling the transfer of knowledge learned from one domain to another. These techniques aim to improve the performance of deep learning models when applied to data from different sources or domains. In the context of mammograms, domain adaptation can enable the development of models that are robust to variations in imaging protocols, equipment, and patient demographics, thereby improving the accuracy and reliability of breast cancer diagnosis [3].

2 Challenges in Mammogram Image Classification

Furthermore, there are several other challenges associated with mammogram image classification. One of the primary challenges is the high inter-observer variability among radiologists, which can lead to inconsistent diagnoses and treatment plans. This can be attributed to differences in expertise, experience, and even personal biases. Additionally, breast cancer can manifest in various forms and can have different characteristics, which makes it challenging to develop a universal model for accurate classification. Moreover, the presence of breast implants or dense breast tissue can also make it difficult to accurately detect and classify abnormalities in mammogram images.

Another major challenge is the lack of diversity in the available datasets for training machine learning models. Many datasets are often biased towards a specific population, such as Caucasian women, which can lead to inaccurate classifications for other populations. Additionally, collecting labeled data for mammogram images can be time-consuming, expensive, and ethically challenging, as it involves exposing individuals to radiation. In addition, different mammography instruments and protocols can produce images with different characteristics, which can affect the accuracy of machine learning models trained on these images (fig. 1.).

Given these challenges, there is a need for more advanced techniques that can improve the accuracy and reliability of mammogram image classification. One such technique is domain adaptation, which has shown promising results in various applications, including medical imaging.

3 Domain Adaptation for Mammogram Image Classification

Domain adaptation techniques can be applied to improve the accuracy of breast cancer classification on mammogram images by adapting models trained

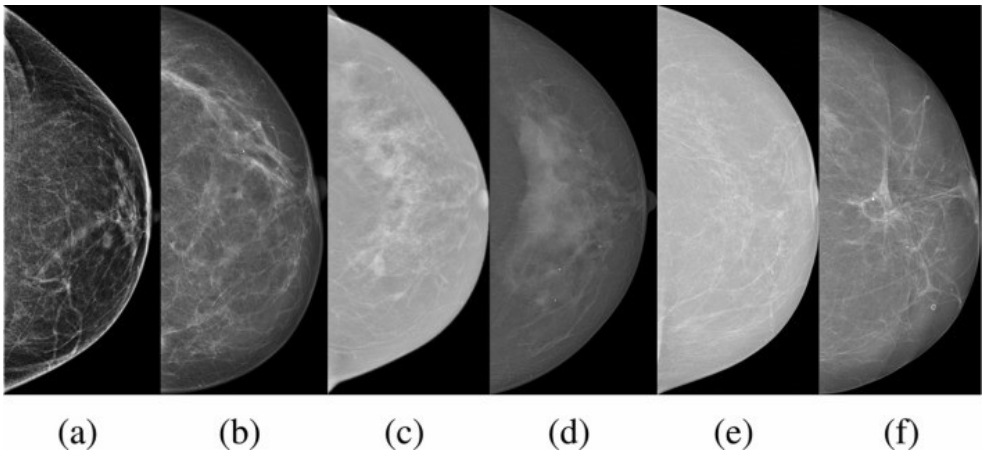

Fig. 1. Sample mammograms from the six domains: (a) OPTIMAM Hologic (b) OPTIMAM Siemens (c) OPTIMAM GE (d) OPTIMAM Philips (e) INbreast and (f) BCDR dataset. [1]

on one dataset to another, without the need for additional labeled data. Domain adaptation aims to transfer knowledge from a source domain (where labeled data is available) to a target domain (where labeled data is scarce or unavailable). In the context of mammogram image classification, domain adaptation techniques can be used to adapt models trained on mammogram images from one population to another, where the distribution of the data may differ in terms of age, ethnicity, or imaging equipment.

3.1 Techniques for Domain Adaptation

Various domain adaptation techniques have been proposed for mammogram image classification, including adversarial domain adaptation, transfer learning, and unsupervised domain adaptation. Adversarial domain adaptation involves training a domain classifier to distinguish between the source and target domains, while the main classifier is trained to minimize the domain shift between the two domains. Transfer learning involves fine-tuning a pre-trained model on the source domain to improve its performance on the target domain. Unsupervised domain adaptation involves learning domain-invariant features that are applicable to both the source and target domains.

4 Conclusion

In conclusion, domain adaptation techniques have the potential to improve the accuracy of breast cancer classification on mammogram images by adapting models trained on one dataset to another, without the need for additional

labeled data. The application of domain adaptation techniques to mammogram image classification can help overcome the challenges of limited labeled data and domain shift, resulting in more accurate and reliable breast cancer diagnosis. Further research is needed to explore the effectiveness of different domain adaptation techniques on mammogram image classification and to develop more robust and accurate models for breast cancer diagnosis.

Acknowledgement. The authors gratefully acknowledge the financial support provided by Agaur FI (Agency for Management of University and Research Grants) for receiving the fund with grant 2022 FI_B 00557. This work was further supported by the following projects: Project TED2021-130081B-C21, Project PDC2022-133383-I00:, and Project PID2019-105789RB-I00.

References

[1] Garrucho, L., Kushibar, K., Jouide, S., Diaz, O., Igual, L., & Lekadir, K. Domain generalization in deep learning based mass detection in mammography: A large-scale multi-center study. *Artificial Intelligence in Medicine*, 132, 102386., 2022.

[2] Wang, Y., Feng, Y., Zhang, L., Wang, Z., Lv, Q., & Yi, Z. Deep adversarial domain adaptation for breast cancer screening from mammograms. *Medical image analysis*,73, 102147, 2021,

[3] Wollmann, T., Eijkman, C. S., Rohr, K. Adversarial domain adaptation to improve automatic breast cancer grading in lymph nodes. *AIEEE 15th International Symposium on Biomedical Imaging, pp. 582-585 2018.*

Understanding ageing patterns: a path to healthy ageing through artificial intelligence

Mary Carlota Bernal *

Department of Computer Engineering and Mathematics, Universitat Rovira i Virgili
Tarragona, Spain
mary.bernal@estudiants.urv.cat

1 Introduction

The planet is changing its population distribution toward more advanced ages, which means that by 2050 the proportion of inhabitants over 60 years of age will double [1]. However, this increase in life expectancy offers various opportunities if healthy ageing is enjoyed, which brings challenges for countries, their populations, and ourselves. We are in the Decade of Healthy Ageing, for this reason, this project investigates how artificial intelligence has been used to study human ageing and from this, uses artificial intelligence for the analysis of population data, with the aim of understanding ageing trajectories based on the concept of healthy ageing of the World Health Organization, which refers to the development and maintenance of functional capacity that allows well-being in old age [1].

This article is organised as follows: Section II describes how artificial intelligence has been used in the study of human aging. Section III describes the approach proposed for the study and the methods used. Finally, the article concludes with some comments about future work.

2 Artificial Intelligence for the study of human ageing

The application of artificial intelligence tools is gradually contributing knowledge to the study of ageing patterns. Table 1 shows the main uses or applications of artificial intelligence in the study of ageing.

Initially, the application of artificial intelligence techniques was more related to the study of age-related differences in gait patterns and understanding of cognitive changes during the ageing process. However, the use of artificial intelligence has recently been centered on the development of biomarkers or "clocks" that can determine a biological or physiological age of an organism. This may be due to the incursion of deep learning techniques used to develop

* PhD advisor: Agusti Solanas, Antoni Martinez

Application	Description
Age-related differences in walking	Automatic recognition of gait changes due to ageing.
Functional properties of brain networks and cognitive changes	Study of changes in the anatomy and function of the human brain that impair many cognitive processes throughout life.
Biological age prediction	Studies that propose biomarkers or aging clocks to study the biological age of individuals.

Table 1. Applications of artificial intelligence in ageing research

age predictors. Artificial intelligence techniques used in the study of aging have been applied to datasets of different types such as data related to hematological or blood biochemistry, gene expression profiles, images, gene expressions, blood chemistry, and physical and mental components based on demographic characteristics, questionnaires, and data on mobility and gait patterns.

The implementation of artificial intelligence techniques occurs through machine learning for the development of different tasks such as classification, regression, and categorisation according to the objective of the model, the types of data, and the approach of the author's strategy to achieve the best benefits. Highlights the use in the different studies of the techniques: support vector machines, artificial neural networks, gaussian process regression, extreme gradient boosting, decision tree, random forest, independent component analysis, linear discriminant analysis, regularized linear regression, and K-Nearest Neighbors. However, neural networks have been major players in developing research in this area. The increase in their application has led researchers to explore other approaches to reduce the variance of models based on neural networks through ensemble learning, training multiple models instead of one, and combining the predictions of these models, which can also result in predictions better than any with a single model.

3 Practical Approach

Functional ability and intrinsic capacity are two terms developed by the World Health Organization (WHO) in the World Report on Aging and Health [2]. According to the WHO, the functional ability is the relationship that occurs between the individual and the environment in which he lives, and how they interact. For this reason, healthy ageing is the process of developing and maintaining the functional capacity that allows well-being in old age. In turn, the intrinsic capacity is the combination of all the physical and mental capacities of an individual expressed through their five key domains (cognitive, locomotor, psychological, vitality, and sensory) [3]; but not only does the ability to carry out the activities determines the functionality of the person, but also the interaction with the environment where he lives. This interaction between

the capacities of the individual and his relationship with the environment constitutes the functional capacity. In accordance with the above, this investigation focuses on the study of functional ability by obtaining a model that allows estimating the intrinsic capacity of the person considering their five key domains (cognitive, locomotor, psychological, vitality, and sensory) and with this to be able to analyze the characteristics of the environment that affect that capacity, all this using national ageing surveys.

3.1 Data Sources for study ageing. Overview

As discussed in the previous sections, the study of ageing requires evidence-oriented approaches based on data, which is usually stored in electronic data sets. For decades, many global initiatives have been dedicated to creating data sets and developing studies to understand ageing processes. Large sets of public data obtained from longitudinal or cross-sectional studies provide essential evidence on ageing processes that are difficult to obtain individually, therefore, analyzing these public datasets it can be observed that several include data related to all domains of well-being indicated by the WHO as part of its definition of healthy ageing [2]: physical, mental, cognitive, social and nutritional; exploiting these datasets is very useful since the result can show valuable information that allows guiding the aging processes toward a healthy path or suggest new methods or variables that must be collected to deepen the results. For the study of functional ability in this research, a population data management strategy is proposed that includes data analysis using the Health and Retirement Study, a longitudinal study of people aged 51 and older and their partners, living in the United States of America [4]. It is important to note that this data source is the reference for the common data collection approach to large-scale longitudinal studies on ageing in the world.

3.2 Proposed Method

A data management strategy has been developed which involves the following stages: collecting, processing, validating, and storing data. This has made it possible to integrate different types of data, harmonize data between the different waves of survey application, and homogenize variables through recognition, mapping, and transformation of the questions survey. All this with the purpose of estimating through key indicators the domains of intrinsic capacity. The evaluation and categorization are carried out following the recommendations of the WHO Integrated Care Guide for the Elderly (ICOPE) [5], as a basis for the quantitative evaluation of the domains of intrinsic capacity based on self-reported questions and assessment tests. Figure 1 presents the design of the strategy used to address the management and analysis of the data, the estimation, and the proposed modeling.

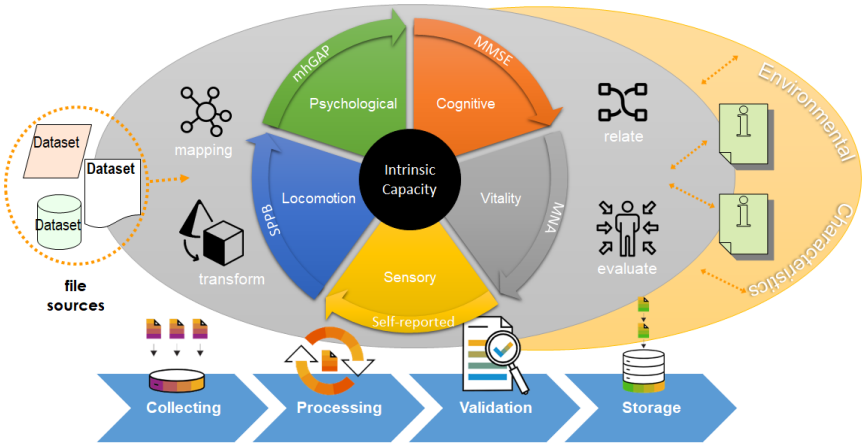

Fig. 1. Data management strategy used for the model. Abbreviations: MMSE, mini mental state examination; MNA, mini nutritional assessment; SPPB, short physical performance battery; mhGAP, mental health gap action programme

4 Conclusion and future work

This project addresses the study of ageing from a perspective that is not focused on the disease, but rather a comprehensive and systemic understanding of ageing with an optimistic vision of its impact. For this reason, It is important to be able to assess intrinsic capacity but also to explore functional ability by analyzing for each domain the structures and body functions, the abilities to carry out activities, and the impact generated by personal and environmental factors on ageing patterns. The use of artificial intelligence as a prospective exercise helps to study these relationships.

References

[1] World Health Organization, "Ageing and health," 2022. [Online]. Available: https://www.who.int/news-room/fact-sheets/detail/ageing-and-health

[2] W. H. Organization, "Ageing: Healthy ageing and functional ability," 2020. [Online]. Available: https://www.who.int/westernpacific/news/q-a-detail/ageing-healthy-ageing-and-functional-ability

[3] M. Cesari, I. Araujo de Carvalho, J. Amuthavalli Thiyagarajan, C. Cooper, F. C. Martin, J.-Y. Reginster, B. Vellas, and J. R. Beard, "Evidence for the domains supporting the construct of intrinsic capacity," *The Journals of Gerontology: Series A*, vol. 73, no. 12, pp. 1653–1660, 2018.

[4] F. T. Juster and R. Suzman, "An overview of the health and retirement study," *Journal of Human Resources*, pp. S7–S56, 1995.

[5] I. WHO, "Integrated care for older people (icope): guidance for person-centred assessment and pathways in primary care," 2019.

Uncovering Maternal Vitamin B12 Status through Unsupervised Machine Learning

Muhammad Mursil *

Department of Computer Engineering and Mathematics, Universitat Rovira i Virgili Tarragona, Spain
muhammad.mursil@urv.cat

1 Introduction

Maternal Vitamin B12 is considered a vital nutrient in the development of a fetus during pregnancy and is associated with short- and long-term effects on neonatal health [1]. Since maternal vitamin B12 for both mother and fetus is associated with many adverse pregnancy outcomes, adequate vitamin B12 status during pregnancy is essential. The adverse outcomes include cognitive and neurological dysfunction, early miscarriage, preterm birth, fetal growth restriction and preeclampsia [2]. The cutoff for Vitamin B12 is below 148 pmol/L, but it is an unreliable indicator for Vitamin B12 deficiency status in pregnancy since there is a gradual physiological decline in Vitamin B12 concentration during pregnancy. It is hypothesized that hemodilution, active transport of Vitamin B12 across the placenta, hormonal changes and Vitamin B12 binding protein concentration alteration all contribute to this decline [3].

This study aims to assess reliable indicators of Vitamin B12 status during pregnancy using unsupervised learning. An unsupervised learning approach could help to determine the cutoff value of maternal Vitamin B12 in pregnancy. It uses machine learning algorithms to cluster unlabeled data, find hidden patterns, similarities and differences in the information, and provide the ideal solution [4].

The standard and most popular unsupervised learning algorithm, K-means clustering, is used to overcome this challenge with clinical parameters such as birth weight (BW), gestational week at birth (GW) and maternal vitamin B12. This study is based on 607 mother-child cases from the two hospitals in the Tarragona region, Spain. The results showed the minimum, medium and maximum cutoff range of maternal vitamin B12. As per our knowledge, this is the first study to use an unsupervised machine learning algorithm to assess the maternal Vitamin B12 status.

* PhD advisor: Prof. Domenec Puig, Prof. Michelle Murphy, Dr. Hatem A Rashwan

2 Methodology

This study used the K-means clustering algorithm to assess a reliable indicator for vitamin B12 deficiency in pregnancy. K-means clustering algorithms were used because it is popular and widely accepted for data segmentation, data exploration, identifying hidden patterns and anomaly detection. The figure 1 shows the workflow of the implemented approach.

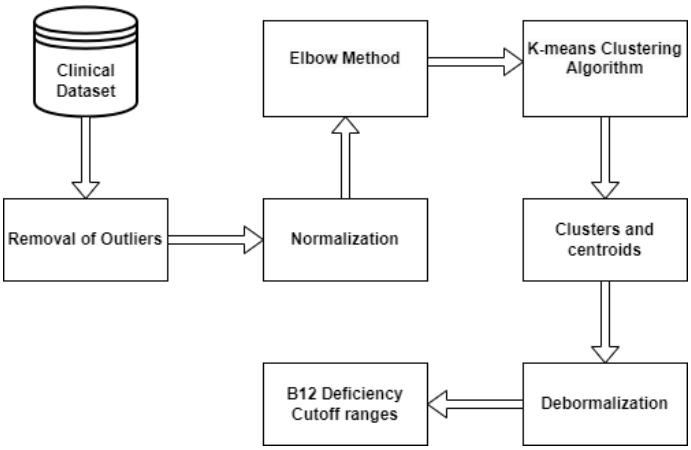

Fig. 1. Proposed approach for this study

2.1 Data Preprocessing:

The clinical data were collected from the birth cohort of the two public hospitals of the Tarragona region, Spain. A total of 783 local pregnant women participated in this study. After removing the incomplete cases and outliers, the analysis was performed on the data of 607 patients with the clinical attributes such as Sex, Birth weight (BW), Gestational week (GW), Maternal Vitamin B12 and Birth weight percentile (BWP).

Detection and Removal of Outliers: The standard Interquartile range (IQR) technique were used to overcome the negative impact of outliers and the poor performance of the K-means clustering algorithm [5].

Normalization: The MinMax Scaler technique was applied to the data to ensure each feature had the same distribution and ranges. It is essential to use normalization to improve the model performance and robustness and reduce over fitting. The formula of MinMax scaler can be represented as

$$\hat{x} = \frac{x - min(x)}{max(x) - min(x)},$$

where x is the input data, and $\hat{x}$ is the normalized data.

An improvement is noticed in the performance after applying the normalization technique.

Elbow method: The elbow method is used in this study to determine the minimum optimal cluster number in the data set. Figure 2 plotting variation shows that three (k=3) is the minimum optimal cluster number in the data set.

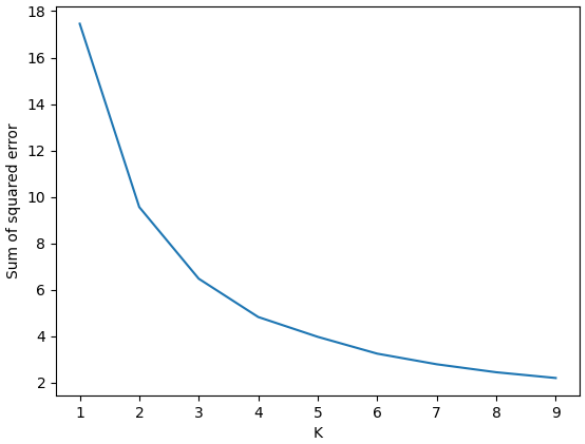

Fig. 2. Elbow method plotting variation

2.2 K-means Clustering:

K-means clustering is the standard unsupervised machine learning algorithm used in this study. K-means clustering does not require labelled data and is used for grouping similar data points in the dataset. For the algorithm to function, it provide several clusters, and each iteration of the algorithm divides the data points into that many clusters. The algorithm starts working by picking k random data points to serve as the cluster's initial centroids. Next, using a distance metric like Euclidean distance, the remaining data points are placed in the cluster that contains the centroid that is closest to them.

After all the data points have been classified, the centroids are revised by averaging the values inside each cluster. Data points are assigned to clusters, and centroids are updated until there is no substantial difference between them.

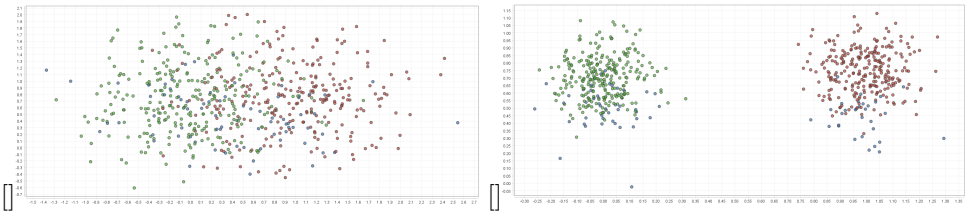

Fig. 3. Data Scatter plot (a) Without clustering and (b) With clustering

3 Experimental Results

The K-means algorithm was employed to determine the indicator of Vitamin B12 deficiency in pregnancy, and the elbow algorithm was used to decide the minimal optimal number of clusters. As per the result of elbow analysis, three clusters (k=3) were used for K-means analysis to determine the lower, medium and highest cutoff of the Vitamin B12 level in pregnancy. The k-means algorithm picked the cluster's initial centroid randomly, and data points of all clinical parameters such as BW, GW, and Vitamin B12 were placed in the cluster that contains the closest centroid to them. Each cluster's centroid is revised in each iteration until all the data points are distributed into three clusters. Table 1 shows the centroiod points of clinical parameters in each cluster.

Table 1. K-means centroid table

Cluster	Vitamin B12	BW	GW
Cluster 0	0.225	0.614	0.732
Cluster 1	0.299	0.303	0.394
Cluster 2	0.496	0.710	0.795

In clusters 1 and 2, Maternal Vitamin B12 showed a direct relation with other clinical parameters, as their centroid points are in the parallel direction. Somehow, cluster 0 centroid points are not in parallel order. The three centroid points of Vitamin B12 indicate the lowest, medium and highest levels of Vitamin B12 in pregnancy. The data points of all clusters were denormalized, and each cluster's mean and standard deviation of Vitamin B12 were calculated to find out the ranges. Table 2 shows the lowest, medium and highest level of Vitamin B12 in pregnancy.

Table 2. Cutoff of Maternal Vitamin B12

Cluster	Maternal Vitamin B12 Cutoff	Level
Cluster 0	267 ± 61	Lowest
Cluster 1	292 ± 96	Medium
Cluster 2	439 ± 88	Highest

Thus, physicians and obstetricians can use the cutoff mentioned in Table 2 for maternal vitamin B12 lowest, medium and highest deficiency indicators while examining pregnant women.

Acknowledgement. The grant for this work is funded by the Generalitat de Catalunya, Agency for Management of University and Research Grants (AGAUR), Spain.

References

[1] P. Lipari Pinto, C. Florindo, P. Janeiro, R. L. Santos, S. Mexia, H. Rocha, I. Tavares de Almeida, L. Vilarinho, and A. Gaspar, "Acquired vitamin b12 deficiency in newborns: Positive impact on newborn health through early detection," *Nutrients*, vol. 14, no. 20, 2022.

[2] I. E. e. a. Vanderjagt DJ, Ujah IA, "Assessment of the vitamin b12 status of pregnant women in nigeria using plasma holotranscobalamin.," 2011.

[3] R. Obeid, A. L. Morkbak, W. Munz, E. Nexo, and W. Herrmann, "The cobalamin-binding proteins transcobalamin and haptocorrin in maternal and cord blood sera at birth," *Clinical chemistry*, vol. 52, no. 2, pp. 263–269, 2006.

[4] S. Shamitha and V. Ilango, "A roadmap for intelligent data analysis using clustering algorithms and implementation on health insurance data," *International Journal of Scientific and Technology Research*, vol. 8, no. 10, pp. 2008–2018, 2019.

[5] H. Vinutha, B. Poornima, and B. Sagar, "Detection of outliers using interquartile range technique from intrusion dataset," in *Information and Decision Sciences: Proceedings of the 6th International Conference on FICTA*, pp. 511–518, Springer, 2018.

Hybrid Recommendation System for Strengthening Cultural Tourism in the Historic Center of Riohacha District

Isabel Arregocés Julio *

Dep. Computer Engineering and Mathematics, Universitat Rovira i Virgili
Tarragona, Spain
Dep. Computer Science and Electronics, Universidad de la Costa, CUC
Barranquilla, Colombia
iarregoc@cuc.edu.co

Abstract

The research project presents a hybrid recommendation system to enhance the tourist experience in the historical center of the Special of the Riohacha-Colombia Special Tourist and Cultural District. The system employs Information and Communication Technologies tools and is designed to contribute to the cultural tourism indicators. The proposed model creates customized tours that align with the tourist's preferences using Machine Learning techniques. The process integrates two techniques to generate personalized suggestions to the user: association rules with the Apriori algorithm and classification.

Keywords: Recommendation systems; Tourism; Rules of association.

1 Introduction

The rise of intelligent tourism recommenders is associated with the need to provide a meaningful user experience, its functionality covers both individual and/or group preferences in the travel plan as well as contextual aspects of the destination. This is possible thanks to the use of Artificial Intelligence techniques [1].

The approach of technological innovation in tourism has captured the attention of many researchers, highlighting the significant impact technology has had on both in tourism and other sectors related to cultural heritage [2]. Some authors [3] suggest that the use and value of travel guides are strongly connected to Information and Communication Technologies (ICT). Recently [4], they have indicated that the digitization of cultural heritage is essential for disseminating knowledge and its enhancement.

* PhD advisor: José Escorcia-Gutierrez and Aida Valls Mateu

The Colombian Ministry of Commerce, Industry and Tourism (MINCIT) recognizes the potential for cultural tourism in the Special Tourist and Cultural District of Riohacha. Despite several points of interest (POI) with high tangible and intangible heritage value, such as emblematic sites and monuments, a marked weakness has been identified in their promotion, with a scarcity of tourism products and limited use of ICT, depriving tourists of significant experiential support during their city tour. This research proposes implementing a hybrid recommendation model that redefines and adjusts the filtering approach, incorporating inputs of various types, including cultural profile, context and user information, to improve the tourist experience. These inputs can be exploited with machine learning techniques to improve the inference system compared to current techniques.

2 Proposed approach

Figure 1 depicts the proposed hybridization model in a sequence of processes. On the left side, personal data and travel information are presented, which are strongly considered by the classification algorithms. Identifying the tourist's profile with the input data suggests a preferred site. The, the Apriori method uses the information about the preferred site to recommend other sites or points of cultural interest that the tourist could visit based on the established rules. In the proposal, the classifiers deliver the antecedent to the system, while the Apriori algorithm works to deliver the consequent.

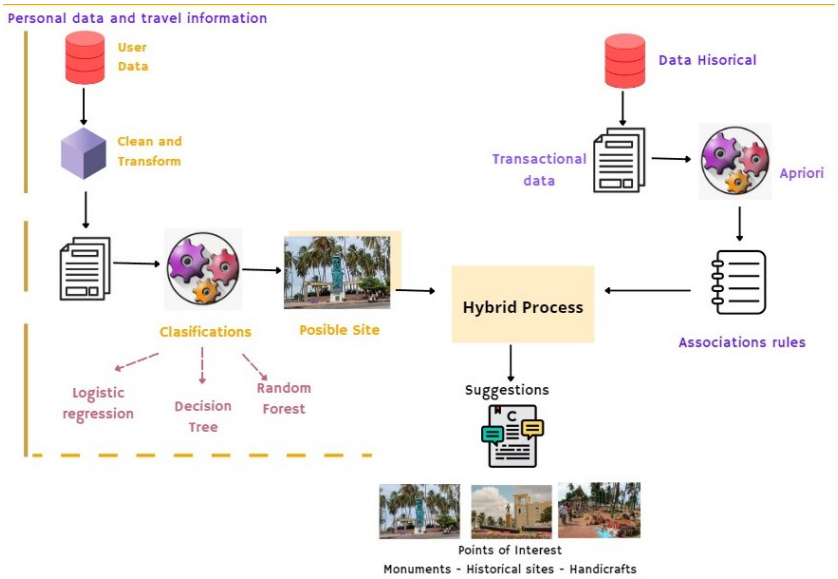

Fig. 1. The proposed workflow for the hybrid recommendation system.

2.1 Dataset

A questionnaire was structured with the help of tourism experts to gather socio-demographic information and visitors' preferences for the District, due to need for more contextual data available. The survey was conducted over three months while tourist visited the points of interest in the Historic Center of the District.

The touristic products offered at cultural sites were analyzed based on MINCIT cultural heritage inventory classification.The personal data collected from 393 tourists are related to: Nationality, place of residence (department), place of residence (municipality), age range, sex, level of studies and occupation; while information on travel preferences is related to the number of sites visited, time spent visiting tourist attractions of cultural interest, accompanying persons and schedule.

3 Results of the association rules

For the creation of these rules, the Apriori algorithm was used [5], this method will allow to extract both frequent items set and association rules that exceed a certain support and confidence. Two essential steps were considered when applying the algorithm:

- Generate frequent itemsets from the database.
- Converting these frequent itemsets into association rules.

Regarding associated tourism products, it was found that the vast majority of tourists visit three to five sites, with a high percentage of them visiting a maximum of six sites. The most frequent items (those with the highest support) were identified within the set of all transactions, see table 1.

Concerning the total number of transactions, the support for each item allowed us to identify that the tourism product 'Handicrafts' has the highest support (83 %), followed by 'Monuments' (62 %).

1 Handicrafts	0.8276836
2 Monuments	0.6214689
3 Culinary Culture	0.5536723
4 Historical Sites	0.5000000
5 Languages and traditional	0.4322034

Table 1. The most referenced tourism products.

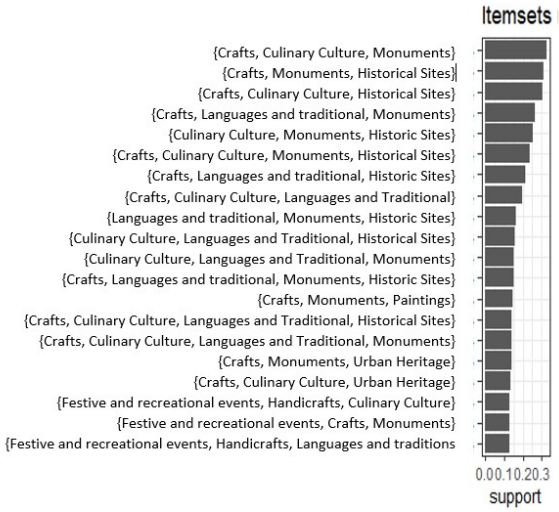

Fig. 2. Associations between the visited places.

4 Conclusions

The preliminary tests performed on the Apriori algorithm for constructing the proposed hybrid recommendation system allowed the identification of preferences for visiting groups of points of cultural interest in the District of Riohacha. A set of association rules have been generated. In future work, we will construct the rest of the recommender system in order to use that association rules to make personalized suggestions to each visitor.

References

[1] J.Borràs, A. Moreno, A. Valls. Intelligent tourism recommender systems: A survey. *Expert systems with applications*, 41(16), 7370–7389, 2014.

[2] A. Cirulis, L. T. De Paolis, M. Tutberidze Virtualization of digitalized cultural heritage and use case scenario modeling for sustainability promotion of national identity. *Procedia Computer Science*, 77, 199–206, 2015.

[3] M. Mieli, M. Zillinger. Tourist information channels as consumer choice: the value of tourist guidebooks in the digital age. *Scandinavian Journal of Hospitality and Touris*, 20:1, 28–48, 2020.

[4] A. Scianna, G. F. Gaglio,, M. La Guardia. Augmented reality for cultural heritage: the rebirth of a historical square. *The International Archives of Photogrammetry, Remote Sensing and Spatial Information Sciences*, 42:303–308, 2019.

[5] R. Agrawal, R. Srikant. Fast Algorithms for Mining Association Rules in Large Databases. Proceedings *20th International Conference on Very Large Data Bases*, Santiago de Chile, 487–499, 1994.

This book contains the proceedings of the 8th Doctoral Workshop in Computer Science and Mathematics - DCSM 2023. It was celebrated in Universitat Rovira i Virgili (URV), Campus Sescelades, Tarragona, on May 3, 2023. The aim of this workshop is to promote the dissemination of ideas, methods, and results developed by the students of the PhD program in Computer Science and Mathematics from URV.

Departament d'Enginyeria [DEIM] Informàtica i Matemàtiques Universitat Rovira i Virgili

Escola Tècnica Superior d'Enginyeria Universitat Rovira i Virgili